Tectonics

RESEARCH ARTICLE
10.1029/2022TC007207

High-Resolution Seismic Imaging of Fault-Controlled Basins: A Case Study From the 2009 Mw 6.1 Central Italy Earthquake

Pier Paolo G. Bruno[1,2], Fabio Villani[2], and Luigi Improta[3]

[1]Dipartimento di Scienze della Terra, dell'Ambiente e delle Risorse, Università degli Studi di Napoli Federico II, Naples, Italy, [2]Seismology and Tectonophysics Department, INGV – Istituto Nazionale di Geofisica e Vulcanologia, Roma, Italy, [3]National Earthquake Observatory, INGV – Istituto Nazionale di Geofisica e Vulcanologia, Roma, Italy

Key Points:

- Five high-resolution seismic profiles image the shallow architecture of the 6 April 2009 (Mw 6.1) L'Aquila earthquake fault hanging wall
- The final images expose the structure of Paganica and Bazzano basins and seismogenic faults dissecting them with unprecedented resolution
- Interpretation of seismic data suggests that Paganica and Bazzano basins have different age, structure, and evolution

Supporting Information:

Supporting Information may be found in the online version of this article.

Correspondence to:

P. P. G. Bruno,
pierpaolo.bruno@unina.it

Citation:

Bruno, P. P. G., Villani, F., & Improta, L. (2022). High-resolution seismic imaging of fault-controlled basins: A case study from the 2009 Mw 6.1 central Italy earthquake. *Tectonics*, *41*, e2022TC007207. https://doi.org/10.1029/2022TC007207

Received 6 JAN 2022
Accepted 14 MAR 2022

Author Contributions:

Conceptualization: Pier Paolo G. Bruno, Fabio Villani
Data curation: Pier Paolo G. Bruno
Formal analysis: Pier Paolo G. Bruno, Fabio Villani
Funding acquisition: Luigi Improta
Investigation: Pier Paolo G. Bruno, Fabio Villani, Luigi Improta
Methodology: Pier Paolo G. Bruno
Project Administration: Luigi Improta
Supervision: Pier Paolo G. Bruno, Luigi Improta
Validation: Fabio Villani, Luigi Improta
Writing – original draft: Pier Paolo G. Bruno, Fabio Villani

Abstract We present the first seismic reflection images of the Paganica and Bazzano basins, two tectonic basins developed in the hanging wall of the Paganica-San Demetrio Fault System, the causative fault of the 2009 Mw 6.1 L'Aquila earthquake, Italy. Five high-resolution seismic profiles were acquired along a main, 7 km long transect cutting across the strands of an active fault system in urbanized areas with widespread sources of seismic noise. Three processing approaches were chosen to tackle a variable and site-dependent data quality. To aid interpretation of this complex setting, we complemented seismic amplitude images with energy and similarity attributes as well with post-stack acoustic impedance inversion. The final seismic sections expose, with unprecedented resolution, the basins' structure and the uppermost splays of the 2009 earthquake. The seismic data show fine details of the subsurface stratigraphic setting, revealing continental depocenters carved in the marine Meso-Cenozoic substratum and displaced by a series of conjugate normal faults, mostly unknown before this study. Several of the imaged fault strands connect to the 2009 coseismic surface ruptures. Matching the seismic interpretation with constraints from surface geology and shallow boreholes, published data from field surveys and scientific drilling, we present a structural map of the Bazzano and Paganica basins with an estimation of the depth of the Meso-Cenozoic substratum. This map highlights a different structure, evolution, and age of the two basins, with the older Bazzano basin that likely began to form in late Pliocene.

1. Introduction

Understanding the structure of fault-controlled extensional basins in active tectonic settings is crucial for the reconstruction of long-term fault activity and for improving seismic hazard assessment. Active normal faults may indeed produce widespread surface faulting during large earthquakes, and shaking may be enhanced by local site effects that usually occur in thick hanging-wall basins filled with low-seismic-velocity sediments. High-resolution seismic exploration of extensional basins has therefore a two-fold goal: (a) to unravel the subsurface location and geometry of faults; and (b) to enable the reconstruction of hanging-wall basin geometry together with thickness and stratigraphic architecture of the depositional infill (e.g., Bruno et al., 2013; Stephenson et al., 2013; Villani et al., 2021).

The central Apennines of Italy are a Neogene fold-and-thrust belt (Cosentino et al., 2010; Malinverno & Ryan, 1986; Vezzani et al., 2010) whose axial zone is affected by post-orogenic extension since the Late Pliocene-Early Pleistocene (Cavinato & De Celles, 1999; D'Agostino et al., 2001; Ghisetti & Vezzani, 1999; Lavecchia et al., 1994). The inner sector of the Apennines belt is one of the most seismically active areas within the Mediterranean region; seismicity is originated mostly by normal faults capable of releasing magnitudes up to ~7, as recorded by both instrumental (Chiarabba et al., 2009) and historical seismicity (Rovida et al., 2011; Tertulliani et al., 2009). Paleoseismic data (Galli et al., 2008), indicate that normal faulting generates the largest-magnitude earthquakes. During the last 100 yr these earthquakes caused more than 35,000 deaths, vast economic losses and widespread destruction only in central Italy. Characterization of active normal faults in the Apennines is however a challenging task, mainly due to the complex structural settings inherited from the superposition of late Pliocene-Quaternary northeast-directed extension onto a contractional stack of thrust sheets that are in turn affected by different sets of Meso-Cenozoic faults (see Patruno & Scisciani, 2021 for a recent review). Moreover, only a few high-resolution multidisciplinary studies have targeted seismogenic normal faults and their associated Quaternary hanging-wall basins (Bosi et al., 2003; Cavinato & De Celles, 1999; Ghisetti & Vezzani, 1999), therefore, we lack key data about geometry, shallow structure, and long-to middle-term slip-rates for many Apennine

Writing – review & editing: Pier Paolo G. Bruno, Fabio Villani, Luigi Improta

faults (see a discussion in Villani et al., 2015). Such data are the foundation for a comprehensive hazard assessment (e.g., Machette et al., 2004).

The need for multidisciplinary studies combining geological field surveys and high-resolution geophysical investigations also arises from mounting evidence of the complex interplay existing between inherited contractional structures, pre-Miocene normal faults and post-orogenic Quaternary extensional fault systems in central Apennines (details in: Barchi et al., 2021; Buttinelli et al., 2021; Pizzi et al., 2017). This complexity poses additional difficulties for active fault detection and characterization. For instance, even the causative fault of the 2009 Mw 6.1 L'Aquila earthquake (Figure 1; D'Amico et al., 2010; Herrmann et al., 2011; Scognamiglio et al., 2010), that is, the Paganica Fault (Bagnaia et al., 1992), was only in part identified prior to the 2009 seismic sequence (Akinci et al., 2009; Boncio et al., 2004; Pace et al., 2006). Since seismic reflection data were unavailable in the mainshock region, the first post-earthquake studies on the mainshock source and on the fault systems activated during the sequence (Cirella et al., 2012; Valoroso et al., 2013) suffered from the poor knowledge of the fault structure in the shallow crust.

To bridge this information gap, geophysical investigations, mostly funded by the Italian Civil Protection Agency, were made in the epicentral area to investigate the subsurface down to a depth of 300–600 m (Balasco et al., 2011; Civico et al., 2017; Improta et al., 2012; Minelli et al., 2018; Pucci et al., 2016). These surveys, together with near-surface microzonation studies (Boncio et al., 2010; Giocoli et al., 2011) and with paleoseismological surveys (Blumetti et al., 2017; Cinti et al., 2011; Galli et al., 2011; Moro et al., 2013), focused on the Middle Aterno Valley, specifically on the Paganica-San Demetrio Fault System, which ruptured during the 2009 mainshock (Figure 1).

Among those target-oriented surveys, a high-resolution seismic experiment was carried out by Improta et al. (2012), which collected two profiles across the Paganica Fault and its hanging-wall basin and three profiles across the Bazzano basin (Figures 1 and 2). These are the only seismic data available to date, and as a whole, the five profiles span over a 7 km long northeast-southwest transect across the ruptured fault and the associated basins (Figure 2). The seismic data were acquired with a dense wide-aperture acquisition geometry (Operto et al., 2004) that provides information suitable for tomographic inversion of first arrivals and for seismic reflection imaging. Improta et al. (2012) used part of the first arrival information from this experiment to produce *Vp* tomographic models and to propose a simplified geological section across the Bazzano basin and the southern part of the Paganica basin. Villani et al. (2017) merged the results of a tomographic inversion with detailed geological field surveys to build a 4 km long section across the Paganica Fault and its hanging wall basin. Villani et al. (2017) recognize a complex system of synthetic and antithetic buried splays, which generally define a half-graben structure controlled by the long-term displacement accrued by the Paganica fault and its main antithetic splay, that is, the Bazzano fault.

Even if the seismic and electric data acquired in the more recent years (Civico et al., 2017 and references therein) have increased our knowledge of the area, those smooth resistivity and *Vp*-velocity models can only resolve the geometry and the internal structure of the basins at the first order. On the other hand, the need for further improving our understanding of the structure and evolution of the Paganica and Bazzano sub-basins is evidenced by the outcomes of a recent well drilled in the Bazzano basin (LAqui-core: Figures 2 and 3: Macrì et al., 2016). Magneto-stratigraphy analysis on core samples provides constraints on the Middle Pleistocene to Recent sedimentation within the basin; moreover, it unravels an unexpected Early Pleistocene age for a relatively shallow (115–151 m deep) lacustrine sequence found in a zone where the velocity model of Improta et al. (2012) suggests that the depocenter is more than 350 m deep. These results imply that the Bazzano basin includes an approximately 200 m thick deeper portion that is still unexplored, and consequently the beginning of continental sedimentation in the study area is certainly older than the age inferred from the cored sediments.

Seismic reflection profiling is the premiere technique used to obtain detailed images of the subsurface, which are ideal for stratigraphic and structural interpretations. In recent years, great technological advancements in the acquisition and processing of high-resolution onshore data have led to a significant increase in the number of successful explorations of continental basins, providing to geoscientists an imaging resolution comparable to that of marine surveying (e.g., Bruno et al., 2017, 2019; Gold et al., 2020; Haberland et al., 2017). In this article, we present the first seismic reflection images of the Bazzano and Paganica basins and bounding faults obtained by applying advanced and target-oriented processing flows to the profiles acquired by Improta et al. (2012). Our goal

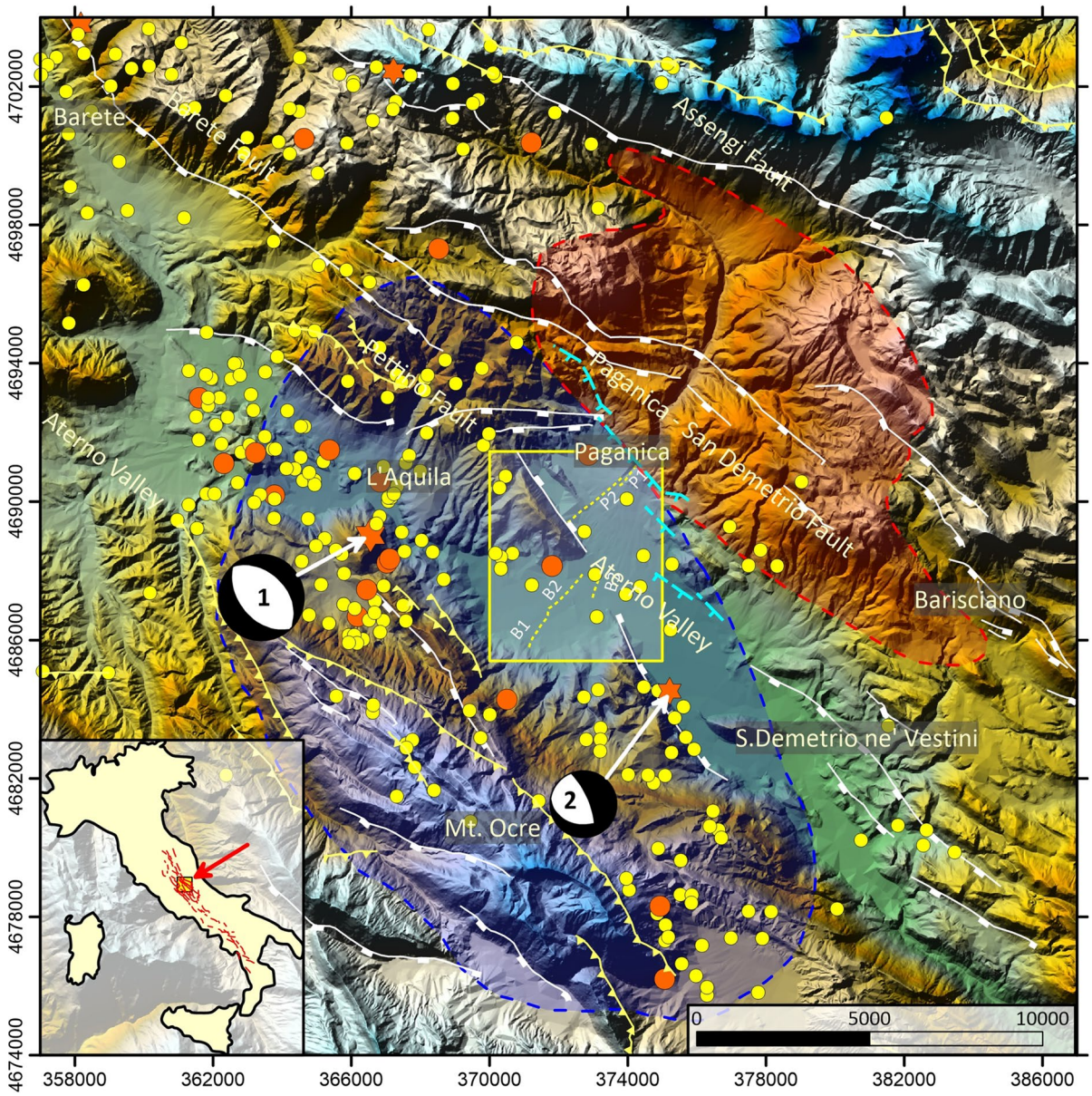

Figure 1. Topographic pattern of the Aterno Valley, central Apennines, and surrounding mountain ranges from a 10 m resolution DEM (TINITALY: Tarquini et al., 2007). In white and pale yellow are normal fault segments and thrusts part of the Aterno Valley and of the central Apennines fault systems. Yellow and orange dots are the epicenters of earthquakes since December 2002 (Mw > 3 and >4 respectively). Orange stars and focal mechanisms are relative to April 6, 2009 Mw 6.1 L'Aquila earthquake mainshock (a) and of the April 7, 2009 Mw 5.6 aftershock (b). Dashed cyan lines are the traces of the coseismic surface ruptures following the April 6, 2009 Mw 6.1 L'Aquila earthquake (Iezzi et al., 2019; Vittori et al., 2011). Blue and red areas are the zones where subsidence and uplift occurred (from DiNSAR analysis: Papanikolaou et al., 2010). Seismic reflection profiles discussed in this article are represented by dashed yellow lines. The yellow box encloses the map shown in detail in Figure 2.

was to obtain detailed images and reliable interpretations of the internal architecture of Bazzano and Paganica basins and of their dissecting faults and recent depositional patterns to shed light on the relations between basins structure and Quaternary faults. In this way, seismic reflection imaging complements the smooth *Vp*-velocity models of Improta et al. (2012) and Villani et al. (2017), which, due to intrinsic limitations of the refraction tomography method (see Supporting Information) can only define the main basin features, despite their relatively high resolution.

We used up-to-date processing and interpretation techniques that are standard for hydrocarbon exploration but not very often seen in shallow onshore exploration. For instance, to improve the seismic interpretation, we merged

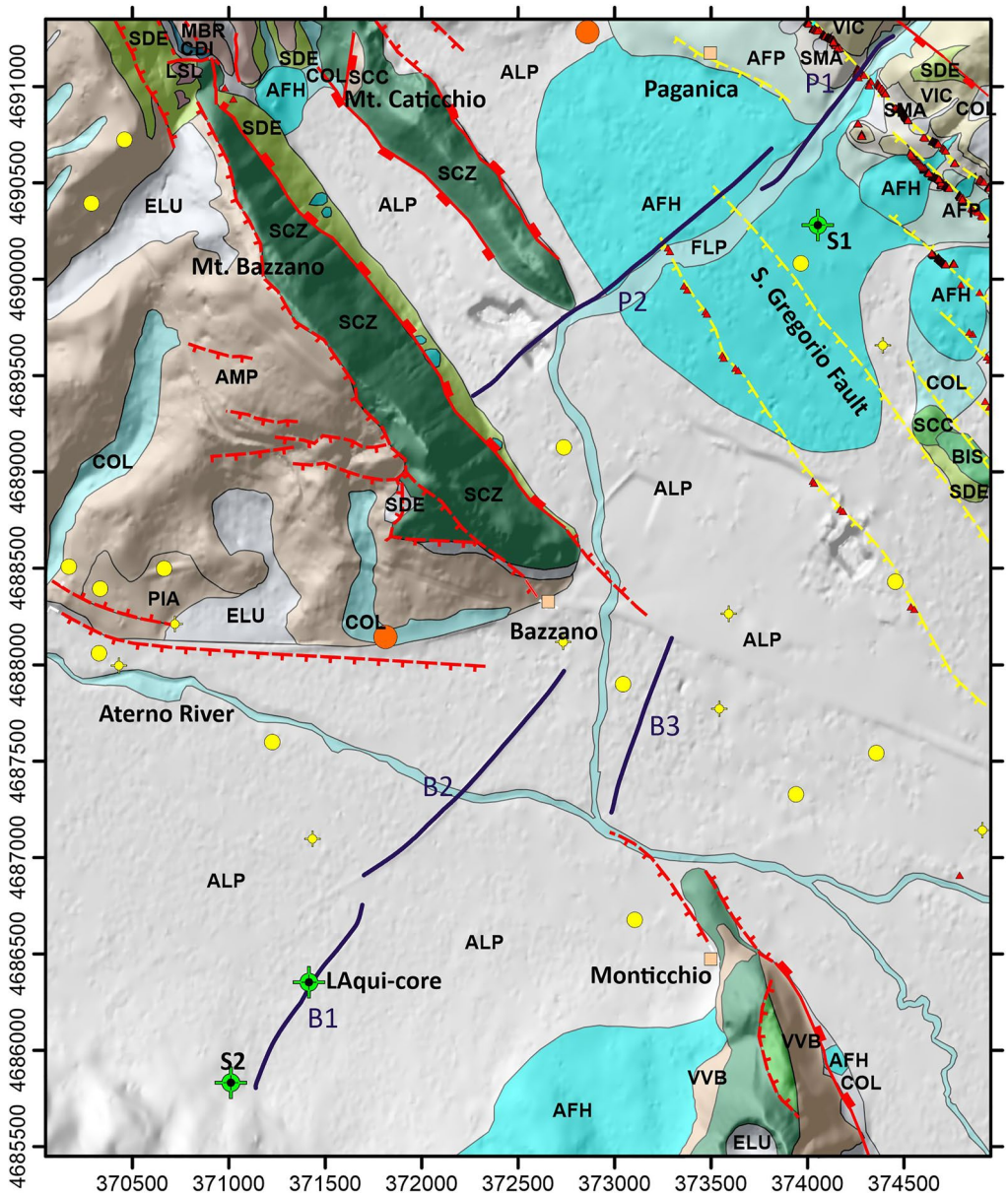

Figure 2. Details of the geological map of the Middle-Aterno Valley, modified from Pucci et al. (2015), overlain to a 10-m-resolution DEM (TINITALY: Tarquini et al., 2007), represented in a greyscale shaded relief, with illumination from northeast. A detailed description of the outcropping geological units is found in Table S1 in Supporting Information S1. Seismic profiles (B1, B2, B3 P1, and P2) are drawn with continuous deep blue lines. Symbols for faults (red), surface ruptures occurred during the 2009 earthquake (yellow, red triangles indicate surface evidence from Boncio et al., 2010; Emergeo Working Group, 2010; Galli et al., 2010) and earthquakes are as in Figure 1. Green circles with cross are the three boreholes (LAqui-core, S1 and S2) used in the interpretation.

classic interpretation methods with seismic attributes and seismic impedance inversion, which are not yet a typical approach in high-resolution shallow imaging of faults, especially in intramontane settings (e.g., Ercoli et al., 2020). These seismic reflection profiles, here presented for the first time, provide subsurface structural constraints to improve our knowledge about the long-term basin evolution. In addition, by integrating results of the seismic surveys with information obtained in recent years by drillings, electromagnetic soundings, and single-station ambient vibration measurements, we propose a structural map of the Meso-Cenozoic substratum underneath both basins. This map may help improve current structural models of the study region.

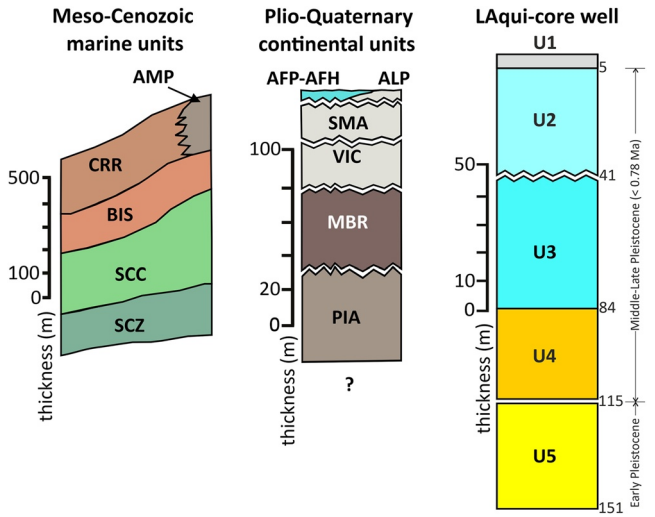

Figure 3. Simplified stratigraphic columns of the Meso-Cenozoic substratum (left) and of the main continental units outcropping in the Paganica area and in the northern part of the Bazzano basin (center: modified and adapted after Pucci et al., 2015). Key to the legend: AFH Holocene alluvial fan; ALP Late Pleistocene alluvial fan; COL, colluvium; ELU, eluvium; SDE, slope debris; SMA, San Mauro Unit (Middle Pleistocene); VIC, Valle Inferno Conglomerates (Early-Middle Pleistocene); MBR, Megabrecce Unit (Early-Middle Plesitocene); PIA, Pianola lacustrine Unit (Late Pliocene-Early Pleistocene); AMP, Miocene Flysch; CRR, Marne con Cerrogna (Miocene); SCC, Scaglia Cinerea Formation (Eocene-Oligocene); SCZ, Scaglia Detritica (Cretaceous-Eocene). Stratigraphy of the LAqui-core scientific drilling (right: redrawn from Macri et al., 2016). U1. Holocene alluvia, U2. Fluvial-alluvial sequence, U3. Palustrine sequence, U4. Alluvial fan gravels (Units 2–4 date back to Middle-Late Pleistocene), U5. Palustrine sequences (Early Pleistocene). Units 2–4 are younger than 780 ka based on magnetic data. Age <460 ka is hypothesized according to the analysis of tephra layers. Unit 5 has been related to the Madonna della Strada Synthem (1.2–1.7 Ma). Thus, a long sedimentation hiatus (1.2–0.46 Ma?) has been hypothesized separating Units U4 and U5.

2. Structural Settings

The L'Aquila earthquake sequence (Chiarabba et al., 2009) hit an internal area of the central Apennines (Figure 1), which endured thrusting during late Miocene, with local out-of-sequence thrusting taking place up to the Early Pliocene, as documented in the Gran Sasso range (details in Ghisetti et al., 1993; Patacca et al., 1990). Subsequently, the chain was affected by Pliocene-Quaternary extension (Cavinato & De Celles, 1999; D'Agostino et al., 2001; Ghisetti & Vezzani, 1999; Lavecchia et al., 1994). This sector of the Apennines is made of Mesozoic-Tertiary carbonate and marly ridges divided by fault valleys hosting Miocene siliciclastic deposits (Bosi & Bertini, 1970; Centamore et al., 2006). The tectonic structure consists of inherited Jurassic-Cretaceous normal faults, which are cross-cut by northwest-trending Miocene-Pliocene thrusts. In addition, the Quaternary extension created a network of northwest-to west-striking normal fault systems (Cowie & Roberts, 2001; Galadini, 1999; Galadini & Galli, 2000; Galadini & Messina, 2001, 2004; Morewood & Roberts, 2000; Roberts et al., 2002, 2004) that in some areas reactivated local pre-existing structures (Pizzi & Galadini, 2009; Pucci et al., 2019).

Paleoseismic investigations along the Paganica-San Demetrio Fault System (Figure 1) confirmed the occurrence of surface-rupturing earthquakes since the Late Pleistocene (Blumetti et al., 2017; Cinti et al., 2011; Moro et al., 2013). This geologic structure belongs to a larger array of Plio-Quaternary faults whose Late Pleistocene-Holocene activity was discovered before the 2009 earthquake (Galadini & Galli, 2000; Galli et al., 2008). The study area encompasses the so-called Upper and Middle Aterno River Fault System, which generated a set of sub-parallel and partly coalescent tectonic depressions late Pliocene-Quaternary in age (Bagnaia et al., 1992; Bertini & Bosi, 1993; Bosi & Messina, 1991; Cosentino et al., 2017; Vezzani & Ghisetti, 1998). In the Middle Aterno River Valley, the 2009 earthquake activated at least three main right-stepping fault segments of the southwest-dipping Paganica-San Demetrio Fault System, producing coseismic ground faulting and fracturing with maximum throws of a few centimeters (see Boncio et al., 2010; Emergeo Working Group, 2010). The majority of the surface breaks occurred along fault strands with cumulative fault scarps several meters high in their footwall and affecting Middle to Late Pleistocene alluvial and fluvial deposits (Galli et al., 2010; Roberts et al., 2010). The hanging wall of the Paganica-San Demetrio Fault System presents significant antithetic structures, such as the Bazzano and Monticchio northeast-dipping normal faults, and a small substratum salient in between (Centamore et al., 2006), both indicative of a complex topography of the Meso-Cenozoic substratum.

3. Characterization of Paganica Fault

Seismologic data well define the geometry, size, and kinematics of the Mw 6.1 mainshock associated with the Paganica Fault (Chiarabba et al., 2009; Chiaraluce, 2012; Cirella et al., 2012). Geodetic studies (Atzori et al., 2009) show that coseismic slip induced a maximum subsidence of ~0.25 m in the fault hanging wall (Figure 1). Lacking crustal seismic profiles, the deep geometry of the mainshock causative fault is inferred exclusively by a main alignment of aftershocks hypocenters (from 2 to 9 km deep), whose geometry is compatible with the surface trace of the Paganica Fault (Chiaraluce et al., 2011; Valoroso et al., 2013).

The Paganica basin is one of the major tectonic depressions developed in the Middle Aterno River Valley. This basin is bounded by the southwest-dipping Paganica-San Demetrio Fault System and by the northeast-dipping Bazzano antithetic fault, and is emplaced on Meso-Cenozoic carbonates of slope to basin successions, late Jurassic to Early Miocene in age (Figures 2 and 3; details in Tables S1 of the Supporting Information). Villani et al. (2017)

found that the Paganica basin is entirely produced by normal faulting. They identified large cumulative fault displacement (~650 m) in the footwall of the Paganica fault, which suggests that the onset of extensional activity occurred in the Early Pleistocene (Gelasian stage, about 2.5 Myr ago). In fact, the results of refraction tomography and of other geophysical investigations (Civico et al., 2017; Villani et al., 2017) suggest that the Paganica basin is filled with about 250 m of alluvial deposits whose top part includes Middle Pleistocene tephra (dated about 460 ka; Galli et al., 2010), as well as some small remnants of lacustrine deposits which might date back to the late part of Early Pleistocene (about 1.3 Ma; Bertini & Bosi, 1993; Giaccio et al., 2012; Pucci et al., 2015), although Macrì et al. (2016) propose that the generation of the Paganica basin took place later than 0.78 Ma.

In comparison to the Paganica basin, Bazzano is deeper, being its continental infill more than 300 m thick, according to Improta et al. (2012). Pucci et al. (2019) report of some recent field evidence that the east-trending normal faults, possibly inherited from previous compressional tectonics and re-activated during Quaternary extension, played a role in the early development of the basin and, basing their line of reasoning on cross-cut relationships with younger northeast-trending faults, they suggest for Bazzano an older inception age with respect to the Paganica depression. The southern part of the Bazzano basin is characterized by outcrops of fine-grained sediments (referred to the lacustrine sands and silts of the Early Pleistocene Pianola Unit by Pucci et al., 2015; Figures 2 and 3) and other terraced deposits, including the Limi di San Nicandro Formation (Bertini & Bosi, 1993), which have been interpreted as remnants of an ancient (>2.5 Ma) and wide lake (Cosentino et al., 2017; Pucci et al., 2019). These lacustrine deposits locally rest on a late Miocene flysch (sandstones and siltstones), which covers a Meso-Cenozoic carbonate series (Centamore et al., 2006; see simplified stratigraphy in Figure 3). Most probably, the Miocene flysch is preserved in the sub-surface of the Bazzano basin, as suggested by a 40 m deep borehole located close to the southern end of seismic profile B1 (S2: position in Figure 2). Moreover, the presence of ancient lacustrine deposits in the sub-surface of the Bazzano basin is proved by the lithostratigraphy, micropaleontological and magneto-stratigraphy data of the 151 m deep L'Aqui-core drilling (Macrì et al., 2016) located in the area of maximum coseismic subsidence (position in Figure 2). By adopting here the labeling of Macrì et al. (2016), the borehole encountered the following main units (Figure 3) from top to bottom:

Unit 1: a 5 m thick Holocene alluvial sequence; Unit 2: a 36 m thick, fluvial-alluvial sequence; Unit 3: a 42 m thick palustrine cycle down to 83 m depth; Unit 4: an alluvial-fan gravel package down to 115 m depth; and Unit 5: another palustrine sequence down to the well bottom.

For the uppermost 15 m of the sequence drilled in the LAqui-core, the authors suggest a sedimentation rate of 0.46 mm/yr. Magneto-stratigraphy analysis indicates an Early Pleistocene age for the topmost portion of the deep lacustrine sequence. The latter portion has been tentatively correlated with fluvio-lacustrine deposits that are widespread in the western sector of the L'Aquila basin, a few kilometers to the west of the study area (Scoppito-Madonna della Strada Unit, inferred age of 1.3–1.8 Ma according to Mancini et al., 2012). Cores from Units 1 and 2 date back to the Middle-Late Pleistocene (<0.78 Ma; Macrì et al., 2016), while erosive contacts between Units 2 and 3 and between Units 4 and 5 indicate the occurrence of significant hiatuses, which have also been documented in similar continental sequences outcropping in nearby sectors of the Middle Aterno Valley (e.g., Giaccio et al., 2012; Pucci et al., 2019, 2015). Therefore, we infer that the averaged long-term sedimentation rate from the whole LAqui-core section is probably much lower (possibly ~0.1 mm/yr) than the rate obtained for the uppermost 15 m of the sequence.

Based on the peculiar coincidence of maximum locus of coseismic subsidence of the 2009 earthquake with the largest thickness of the basin infill, Macrì et al. (2016) inferred that the Bazzano depression represents the long-term byproduct of the L'Aquila earthquake fault activity. Concerning the large-scale structure of this depression, in the northern part Pucci et al. (2015, 2019) suggest the occurrence of a main west-trending normal fault at the southern edge of Mt. Bazzano (Figure 2), whereas the southern side of the basin does not show clear evidences of normal faults. Immediately to the southwest of the study area, a series of late Miocene northwest-trending thrusts of the Mt. Ocre tectonic Unit (Figure 1) bound a large part of the Aterno Valley (see also Baccheschi et al., 2020).

Overall, Pucci et al. (2019) and Villani et al. (2017) proposed that the onset of extension in this part of the central Apennines is Early Pleistocene or even older, in accordance with the long-term geomorphic evolution of the Middle Aterno Valley. Conversely, no evidence of compressional tectonics has been detected in the outcropping continental deposits (see Bagnaia et al., 1992; Bertini & Bosi, 1993; Cosentino et al., 2017; Pucci et al., 2019),

Table 1
Acquisition Parameters, Length and Elevation Information for the Five Seismic Profiles

Profile	Arrays	Vib.points	Max fold	n.traces	Geoph/array	Lenght	Min elev	Max elev	Crooked
B1	1	112	108	24,192	216	1,061	588	596	Yes
B2	2	104	82	22,464	216	1,494	587	589	Yes
B3	1	192	89	36,864	192	960	583	592	Yes
P1	1	113	114	23,843	211	1,058	645	679	Yes
P2	3	205	132	42,025	205	2,034	604	647	Yes

which led the aforementioned authors to conclude that the generation of the Middle Aterno valley is solely related to extensional tectonics.

4. Data and Methods

The seismic data set used in this article consists of five high-resolution seismic profiles: two (P1 and P2 in Figure 2) acquired in the Paganica basin and three (B1, B2, and B3 in Figure 2) in the Bazzano basin. The profiles have a cumulative length of 6,800 m and were acquired by Improta et al. (2012) during a two-week-long experiment in 2010. They are overall characterized by a variable data quality. Bazzano profiles B1 and B2 have a better signal-to-noise ratio and less logistical restrictions than B3, whereas at Paganica high urbanization with pervasive anthropic sources of seismic noise heavily affected the signal, especially for P1 that crosses the Paganica village. Lower seismic data quality at Paganica is also due to unfavorable local geological conditions (thick and widespread coarse, clastic deposits causing strong scattering). Of course, this different data quality influenced the processing steps and the final image quality.

All seismic profiles have a northeast to north-northeast trend and, as a whole, they define a transect across the central part of Middle Aterno River valley (Figures 1 and 2). Lines B1 and B2 cross the south-western and central part of Bazzano, between the eastern slopes of the Mt. Ocre calcareous massif and the western slope of the Bazzano-Monticchio ridge. These profiles were acquired above recent fluvial sediments for a length of 1,061 and 1,494 m (Table 1). Line B3 is 960 m long and it intersects the Bazzano ridge at its southeast termination (Figure 2). Profile P2 covers the western portion of the Paganica basin in the hanging wall of the Paganica Fault, running for 2,034 m over Late Pleistocene-Holocene alluvial fan deposits. The southwest end of line P2 stops against Mt. Bazzano fault, while the other end is ∼200 m apart from the lower splay of the Paganica Fault ruptured in 2009 and reported by Galli et al. (2010). Finally, line P1, 1,058 m long, was designed to intersect the main splay of the Paganica Fault. P1 and P2 are spaced ∼100 m apart and overlap for 230 m.

The main acquisition features of the five profiles are summarized in Table 1. Seismic data were acquired by 192- to 216-channel arrays consisting of 4.5 Hz vertical geophones at 5 m station spacing. Data were recorded with a sampling rate of 1 ms and a record length of 16 s and were digitized by a distributed, 24-bit Geode® acquisition systems manufactured by Geometrics Incorporated. A high-resolution vibrating source (IVI-MiniVIB) released at each vibration point an energy of ∼27 kN distributed over a window of 15 s and over a linear frequency range of 5–200 Hz. Vibration points are on average spaced between 5 and 10 m within the geophone arrays, whose lengths are overall from 3 to 10 times larger than the depth of the basin substratum estimated by seismic tomography surveys (from 100 to >300 m; Improta et al., 2012; Villani et al., 2017).

The acquisition parameters ensured a high Common-Mid-Point (CMP: Figure S1 in Supporting Information S1) redundancy, which is critical to increase the signal-to-noise ratio in the stacked data. Elevation differences also affect the final quality of the CMP stacks. Overall, B1 and B2 and, to a certain extent, B3 are characterized by modest elevation variations (Figure S1 in Supporting Information S1), while the largest differences are found along P1 and P2. Four representative common-shot gathers selected from the five profiles illustrate the overall quality of the seismic data in Figure S2 in Supporting Information S1. As discussed, B1 and B2 show the best signal-to-noise ratio, while data from P1, P2, and B3 are instead characterized by an overall lower ratio, especially at large offsets, where many traces had to be removed to preserve a reasonable data quality. Offset reduction as well as poor signal-to-noise ratio affected the quality of the final images for the Paganica profiles and, to a minor extent, profile B3. The shot gathers in Figure S2 in Supporting Information S1 also show that the data are affected

by large static problems, which bend the reflected phases and the first arrivals. Therefore, refraction static corrections played a major role in the processing.

The reflection processing sequence, which is detailed in the supplementary information, was designed to account for the different data quality. Therefore, we produced: (a) depth converted CMP stacks for the Paganica profiles; (b) post-stack time migrated and depth converted images for the Bazzano profile B3 and (c) pre-stack time migrated and depth converted images for the higher-quality profiles B1 and B2. With the purpose of assisting the structural interpretation we computed the "energy" and "similarity" attributes on the post-stack data (Figures 4–6) using dGB Earth Sciences' OpendTect Pro®. Seismic attributes, which are a common tool in hydrocarbon exploration, have been also used in recent years to improve detection of seismogenic faults in complex onshore crustal settings (see Bruno et al., 2017, 2019; Ercoli et al., 2020). "Similarity" is a typical discontinuity attribute that returns trace-to-trace similarity properties in post-stack data (Marfurt et al., 1998). Discontinuities in a seismic volume or section, such as faults or fractures, appear as regions of low similarity (i.e., in black in Figures 4c–6c). Therefore, this attribute is most often applied to highlight possible zones of faults/fractures.

The other attribute we used is the "energy" attribute, which is defined as the squared sum of the sample values in a time or depth-gate (in our case a depth-gate of 10 m, corresponding to 10 samples) divided by the number of samples in the gate. The energy attribute is a measure of reflectivity strength within the chosen time or depth gate. It is therefore useful to detect changes in acoustic impedance and thus relates to lithology, porosity, and thin-bed tuning (Chopra & Marfurt, 2005). We used it to highlight major sequence boundaries, unconformities and to spot major changes in depositional environments and in lithology. Lateral changes of this attribute can indicate faulting, especially if those changes are spatially correlated to discontinuity attributes, such as the similarity (see Figures 4c–6c).

Profiles B1 and B2 were also used for a post-stack acoustic impedance inversion (see the details in the Supporting Information) that was implemented on Landmark's SeisSpace. In many geological environments, acoustic impedance has a strong relationship with petrophysical properties such as porosity, lithology, and fluid saturation (Latimer et al., 2020). The geology of the Bazzano depression is better suited for this analysis because, as discussed in the previous paragraph, the LAqui-core drilling shows the presence of both coarse-clastic alluvial and clayey lacustrine/palustrine sequences in which strong porosity variations are expected. Post-stack inversion of acoustic impedance has been proven successful, particularly in settings where a unique relation between acoustic impedance and porosity can be established, and therefore it is widely used by the petroleum industry as a quantitative approach to determine rock properties from seismic data. Conversely, post-stack seismic impedance inversion so far has rarely been used to characterize shallow onshore structures. Moreover, since acoustic impedance is a layer property, while seismic amplitudes are layer boundaries attributes, acoustic impedance can make sequence stratigraphic analysis more straightforward (Buxton Latimer et al., 2000). As wavelet side lobes are attenuated, acoustic impedance contains all the information present in the seismic data without the complicating factors caused by wavelets, thus eliminating unnecessary complexity in the seismograms.

The inversion process to compute impedance is split in two parts: first, full-bandwidth reflectivity (Figure 7a) is estimated from stacked data, which are assumed to be representative of the band-limited reflectivity sequence (Levy & Fullagar, 1981); second, reflectivity is converted into acoustic impedance (Figure 7b) by integrating the reflectivity functions and by applying statistical stabilization operators to the estimated low frequencies which are missing in the input data (Galbraith & Millington, 1978). Rock density is needed to compute acoustic impedance: in absence of direct measurements, we estimated density from seismic velocities using the Gardner et al. (1974) empirical relationship, which was derived from a series of controlled field and laboratory measurements of brine-saturated rocks, excluding evaporites, from various locations and depths.

We used both results (i.e., the intermediate full-band reflectivity and the final acoustic impedance) to make our interpretation more robust. The full-band reflectivity is overall well correlated with the energy attribute (compare Figure 7a with Figure 4c); however, it provides an added value to the structural interpretation since reflectivity, differently from energy, preserves information about the polarity of the event. As it will be explained more in detail in the next paragraphs, full-band reflectivity (Figure 7a) was used as a guidance to trace geological boundaries, and to better constraint fault interpretation. Acoustic impedance was instead used to discriminate low-porosity lacustrine deposits from higher-porosity alluvial fan and fluvial sediments.

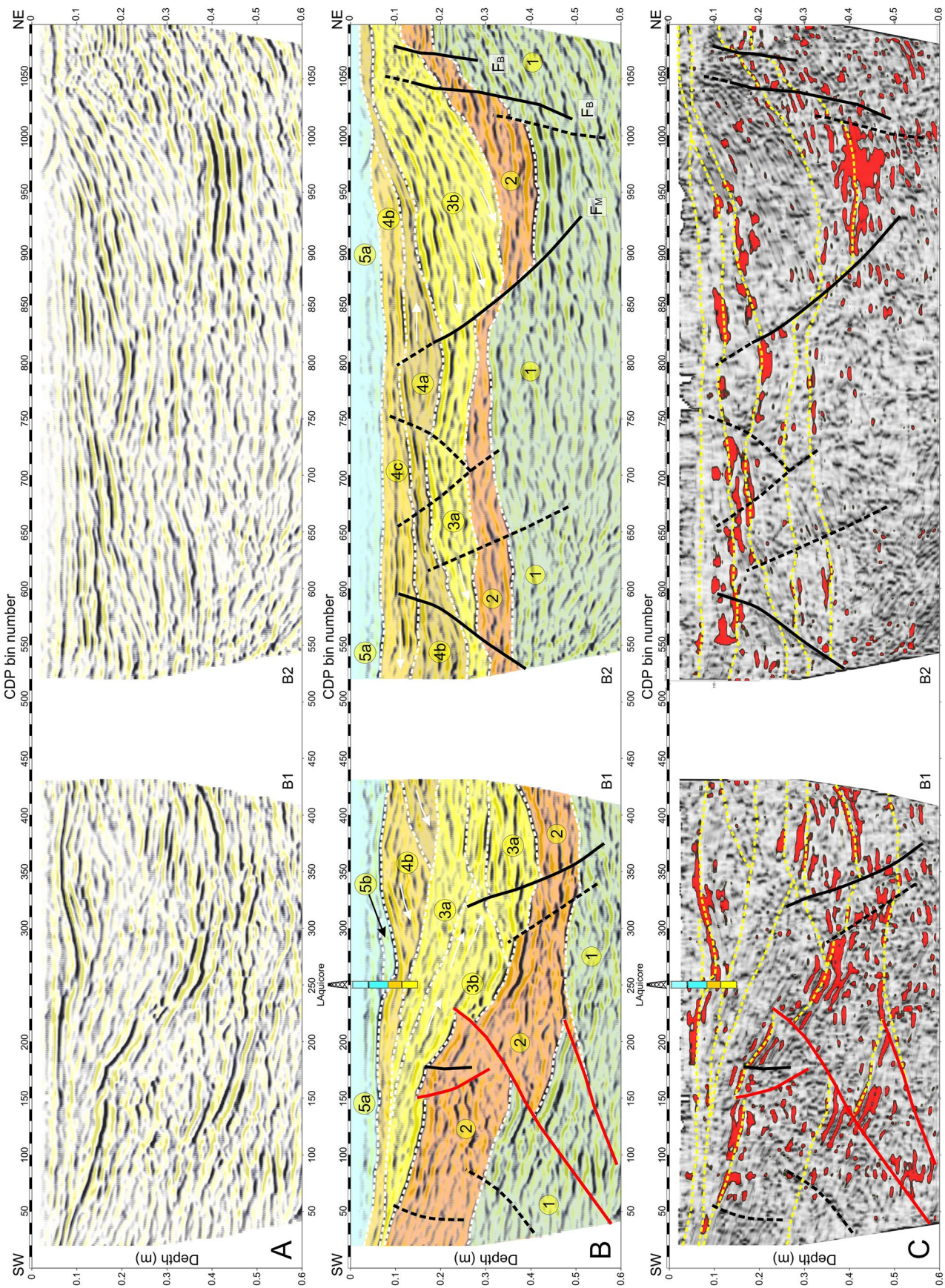

Figure 4. (a) Pre-stack time migrated & depth converted crooked seismic profiles B1 and B2 with (b) superimposed structural and stratigraphic interpretation. In black are the normal faults while in red are the reverse faults. LAqui-core well is intersected at CMP 250. The symbols in yellow circles refer to the stratigraphic units described in Table 2 (c) Plot of similarity attribute (gradational gray palette; black highlight areas of the profiles with the lowest similarity) and energy attribute. In red areas with energy >80%. Energy values <80% are invisible.

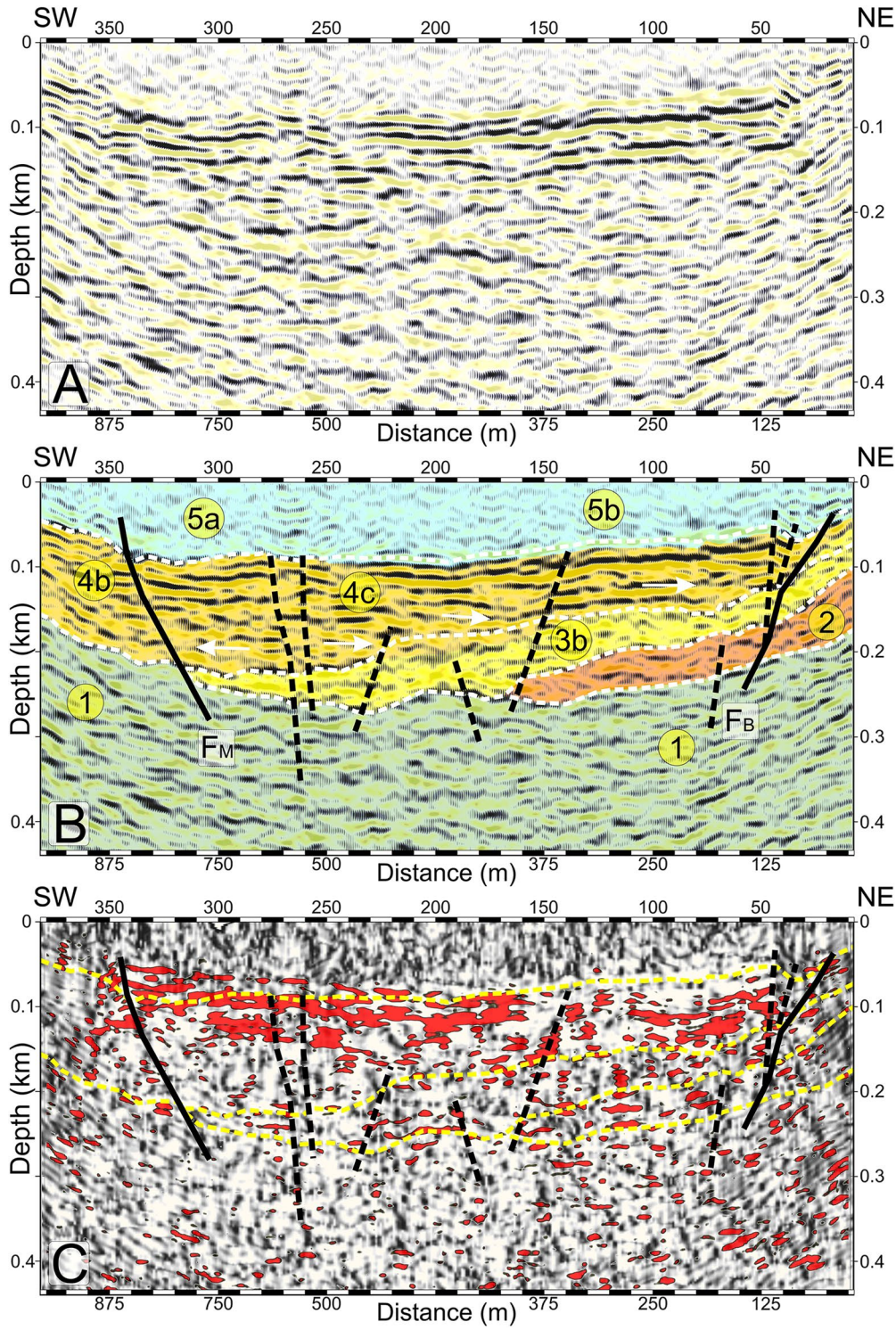

Figure 5. (a) Post-stack time migrated & depth converted crooked seismic profile B3 with (b) superimposed a structural and stratigraphic interpretation. (c) Plot of similarity attribute and energy attribute. Color palettes and symbols are as in Figure 4.

5. Seismic Interpretation

Lacking deep boreholes and related geophysical logs, our interpretation takes into account the recent geophysical surveys targeting the Middle Aterno Valley (e.g., Boncio et al., 2010; Cesi et al., 2010; Civico et al., 2017; Pucci

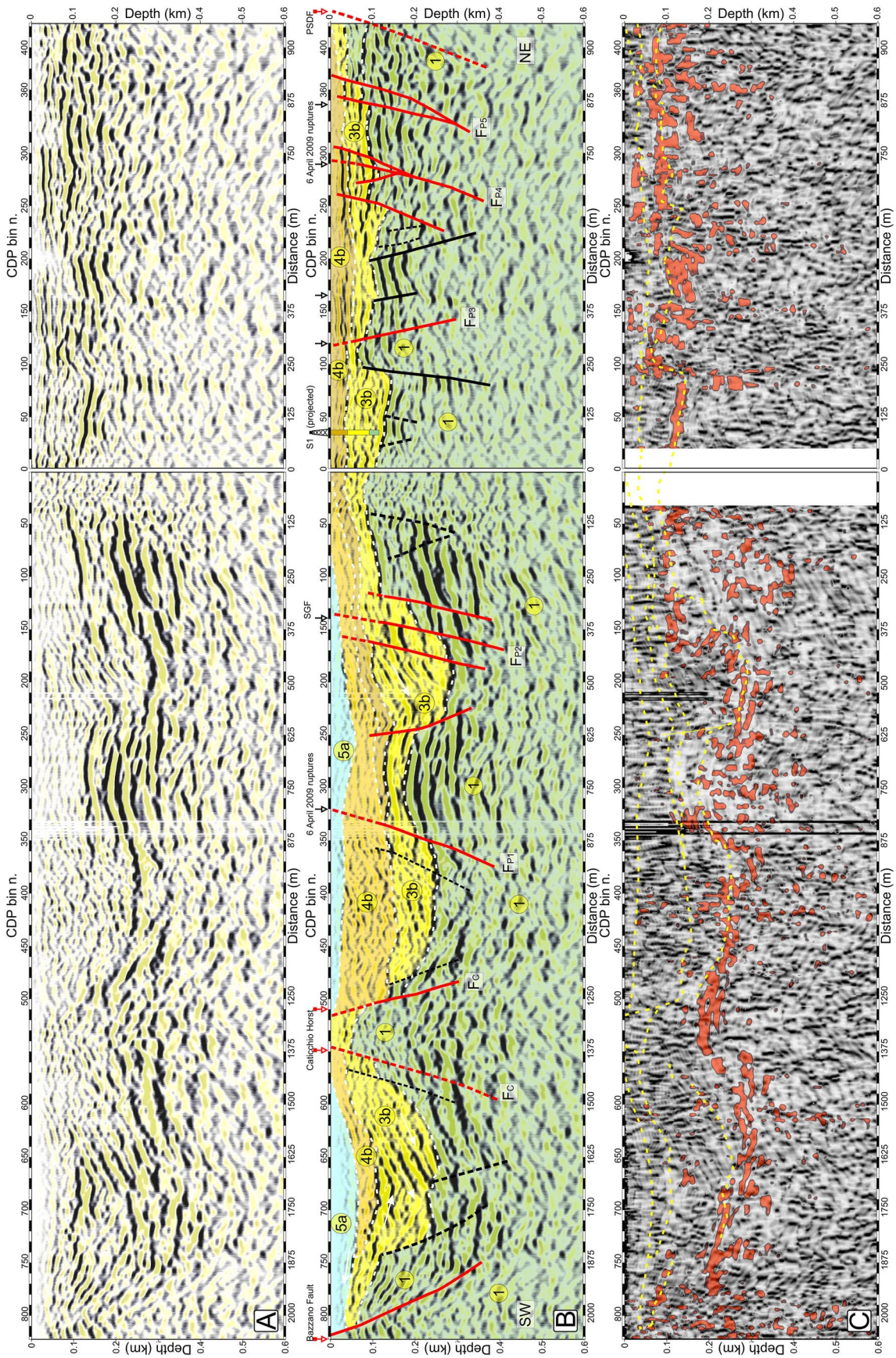

Figure 6. (a) Depth-converted crooked seismic profiles P1 and P2 with (b) superimposed a structural and stratigraphic interpretation. In red are the faults that correlate with surface ruptures and/or mapped faults (see Figures 2 and 8). F_C is Mt. Caticchio bounding faults, PSDF Is the Paganica-San Demetrio Fault system; F_{P1}, F_{P3}, $F_{P4,}$ and F_{P5} are connected with the mapped faults (red arrows) and with the April 9, 2009 ruptures (black arrows); F_{P2} connects to the San Gregorio Fault (SGF). Borehole S1, located ~320 m to the southeast (see Figure 2) is orthogonally projected on the seismic profile at CMP 35. (c) Plot of similarity attribute and energy attribute. Color palettes and symbols are as in Figure 4.

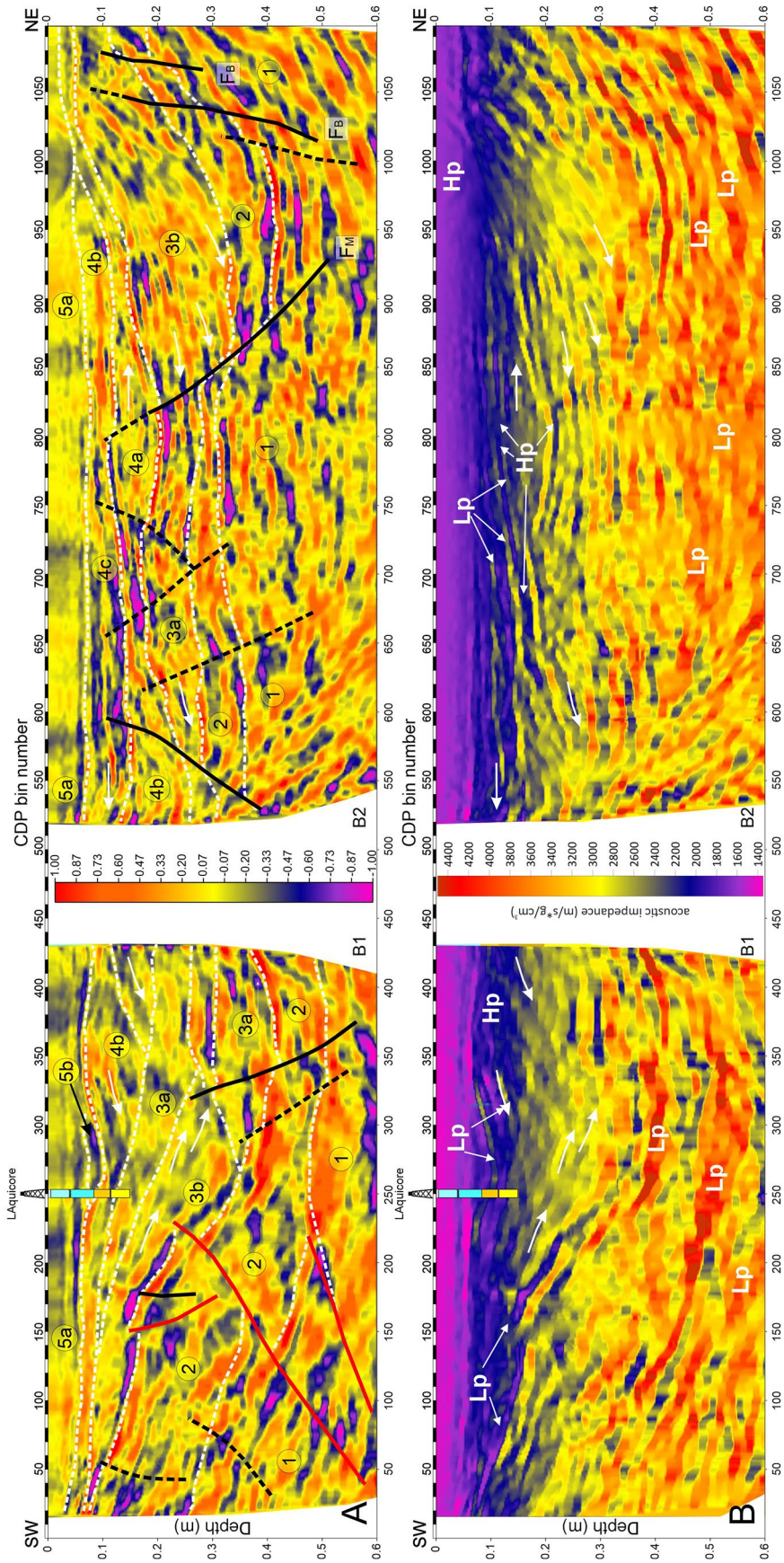

Figure 7. Results of post-stack acoustic impedance inversion on profile B1 and B2: (a) full-bandwidth reflectivity, estimated from the stacked data of Figure 4a with, overlain, the structural and stratigraphic interpretation of Figure 4b. (b) Absolute acoustic impedance ($m/s^*g/cm^3$) obtained by integrating the reflectivity functions and by applying statistical stabilization operators (Galbraith and Millington, 1978) see text; Labels: Lp, low-porosity; Hp, high-porosity.

Table 2
Reflection Characteristics of the Stratigraphic Units Interpreted in the Seismic Profiles and Tentatively Correlated With the Outcropping Units in Figure 2 (Symbols of the Geological Units in the Last Column Are From Pucci et al. (2015) and Are Described in Table S1 in the Supporting Information S1) and With Well Stratigraphy Data (See Macrì et al., 2016)

Unit	Lithology/ environment	Inferred age	Upper boundary	Lower boundary	Internal configurations	Amp.	Cont.	Freq	Correlated outcrops/ wells
5	a) fluvial, alluvial fans	Holocene to	n.a.	Onlap, concordant	Parallel	F L	F L	H F	ALP, AFH, FLP, AFP, ELU, COL, SDE
	b) lacustrine/ palustrine	Late Pleist.			Onlap, parallel	F	F H	VH H	Aquicore
4	a) alluval	Middle Pleist.	Erosional, onlap	Concordant, onlap	Onlap, parallel	H VH	H VH	F L	AFP, SMA
	b) alluvial fans, breccia		Toplap, erosional	Downlap	Sigmoid, prograd.	H F L	H F	F L	VIC, S1, Aqui-core
	c) lacustrine/ palustrine		Concordant	Onlap	Onlap, parallel	H	VH	H	Aquicore
3	a) lacustrine, alluvial	Early Pleist. to	Concordant	Onlap	Onlap, parallel	H F	H F	H F	Aquicore
	b) slope debris & alluvial fans	Late Pliocene	Toplap, erosional	Downlap	Divergent, oblique	F L	H F	H F	MBR, VVB
2	Calcareous-arenaceous	Upper Miocene	Erosional	Concordant	Parallel	F	F H	L	AMP
	Flysch					F L	F	L	
1	Marly-carbonatic	Miocene to Giurassic	Erosional	n.a.	Parallel	VH	F H	L	SCC, SCZ, CCD, CDI
	Sequence					H F	L	L	

Note. Classification of seismic facies follows Emery and Myers (1996). Reflection character (i.e., Amplitude, Frequency and Continuity) has been classified by the following acronyms: VL, very low; L, low; F, fair; H, high, VH, very high.

et al., 2016), in particular the seismic tomography surveys carried out on the B1-B2 and P1-P2 lines (Improta et al., 2012; Villani et al., 2017). Moreover, we consider the litho-stratigraphic information provided by the LAqui-core drilling intersected by profile B1 (Macrì et al., 2016) and two additional, shallower boreholes near the other profiles (S1 and S2: Civico et al., 2017). The detailed geological mapping and stratigraphy published in recent years (e.g., Boncio et al., 2010; Giaccio et al., 2012; Lavecchia et al., 2012; Pucci et al., 2015, 2019 and references therein) is also accounted for. The main reflection characteristics of the five seismic profiles can be seen in Figures 4a–6a. Enlargements of the seismic profiles B1 and B2 for the Bazzano Basin and P1 and P2 for the Paganica Basin are provided in the Supporting Information (i.e., Figures S4–S7 in Supporting Information S1) to allow the reader to better visualize the details of the seismic features discussed here.

The energy and similarity attributes (complemented for profiles B1 and B2 by full-bandwidth reflectivity and acoustic impedance), were heavily used to support and validate the classical interpretation schemes used to locate faults and to define the stratigraphic units, which are mainly based on the visual analysis of reflector offset, reflection internal configurations and reflection character (Table 2).

To identify stratigraphic unconformities (that are known to be characterized usually by large impedance contrast) we followed the peaks of the energy attribute and/or the maxima/minima of the full-bandwidth reflectivity and we spatially correlated them with reflector terminations on the seismic sections. To delineate instead the main fault zones, we looked for lateral changes of the energy attribute and/or of the full-bandwidth reflectivity, and we checked if these features intersect alignments of low similarity and correspond with evident reflector offset on the seismic sections. An example of this approach can be seen by comparing the interpreted boundaries and faults for B1 and B2, which are overlain to the above-mentioned attributes in Figures 4c and 7a.

The high-resolution character of the seismic data allowed the imaging of small-offset faulting. The near-surface of the seismic images, being characterized by a *P* wave velocity of about 1,500 m/s and a dominant frequency of 100 Hz has a vertical resolution limit below 4 m. As the seismic velocity increases and the dominant frequency decreases, vertical resolution drops to 10–12 m in the lower part of the images.

Table 2 summarizes the main characteristics of five seismo-stratigraphic units that we have recognized. The reflection character of these units is variable along the seismic lines, coherently with the large heterogeneity of the geological formations imaged by the seismic profiles and shown by the outcrops near the Middle Aterno Valley. Nevertheless, each of the five Units shows characteristic reflection features, and are found to be coherent in all lines.

In agreement with the available geological information, we interpreted Unit 1 as an undifferentiated Late Jurassic/Cretaceous to Miocene marly carbonatic marine sequence: Scaglia Detritica Formation (SCZ in Figure 2: ∼200 m thick); Scaglia Cinerea Formation (SCC in Figure 2: ∼250–350 m thick); Bisciaro Formation (BIS, outcropping to the northeast and to the southeast of Paganica village, not visible in Figure 2: ∼150 m thick). This interpretation is corroborated by the tomography results of Improta et al. (2012) and Villani et al. (2017), superimposed onto the seismic reflection data in Figures S8–S9 in Supporting Information S1. The comparison shows that Seismic Unit 1 is overall characterized by *P*-wave velocities >4,200 m/s. These high velocities are typically associated with moderate-to low-permeability limestones (see Gardner et al., 1974; Gregory, 1977; Veeken, 2007; Villani et al., 2021). An overall low reflectivity characterizes Unit 1, even if areas at higher reflectivity are present (i.e., profile B2: CMPs 900–1050). The top of Unit 1 appears as a strong and discontinuous reflective event made of few cycles of low frequency and generally at high energy (e.g., Figures 4c and 6c). Locally, it shows seismic features of unconformity with the overlying Unit 2.

Unit 1 is covered by a more reflective package, labeled as Unit 2 and characterized by *P*-wave velocities ranging from 2,200 m/s to 4,200 m/s (Figures S8–S9 in Supporting Information S1; Improta et al., 2012; Villani et al., 2017). Thickness of this Unit is variable and it is recognized only across the Bazzano profiles. Based on tomographic velocities, reflection configurations and presence of an unconformity between Units 1 and 2 we associate Unit 2 with Late Miocene marly limestones and arenaceous flysch (labeled as AMP in Figure 2) outcropping on the southern slope of Mt. Bazzano. This association is also supported by borehole S2, located 150 m to the west of the southern termination of line B1 that penetrated the Miocene flysch at 20 m deep. Unit 2 is ∼90–100 m thick in the central part of the Bazzano sub-basin and more than 200 m thick underneath its south-western margin. Mostly parallel to sub-parallel internal configurations characterize this Unit, even if locally chaotic and non-reflective areas are also visible. Such chaotic parts are consistent with the occurrence of soft-sediment structures visible in many flysch outcrops to the north of Mt. Ocre. The top of Unit 2 is generally seen as a high-energy and fairly continuous reflector, which is interpreted as an unconformity with the overlying reflective packages. Together, Units 1 and 2 constitute the Meso-Cenozoic bedrock within which both the Bazzano and Paganica basins are carved.

A continental sequence, possibly spanning from the Early Pleistocene to Holocene time interval (Units 3–5) fills the basins and overlies unconformably above the basement Units 1 and 2. It shows a large lateral heterogeneity as perceived by the analysis of the seismo-stratigraphic features. Large lateral heterogeneities are also consistent with strong lateral changes of *P*-wave velocity occurring within these units (Figures S8 and S9 in Supporting Information S1; see also Improta et al., 2012; Villani et al., 2017). *P*-wave velocities range from very low values, such as 600 m/s that are typical of near-surface, loose to poorly consolidated alluvia to more than 3,000 m/s, indicative of well-cemented alluvial fan conglomerates and breccia. The Units 3–5 exhibit both propagational internal configurations, typical of fluvial sediments and alluvial fans, and onlapping features indicative of low-energy, lacustrine/palustrine sedimentation. Reflection character also shows a high variability: areas with high-frequency and high-amplitude reflections alternate to zones with low amplitude, low frequency, and low lateral continuity. Downlapping and onlapping terminations are indicative of widespread depositional hiatuses which are confirmed in nearby outcrops of these sequences (Pucci et al., 2015: Figure 2) and by borehole stratigraphy (see Figure 3, Macrì et al., 2016). In the Paganica basin, following the stratigraphic schemes reported by Pucci et al. (2015), these outcropping units comprise (Table S1 in Supporting Information S1): Early Pleistocene chaotic breccia (VBB and MBR) and Early-to-Middle Pleistocene alluvial fan conglomerates (VIC); Middle-to-Late Pleistocene lacustrine silts and sands (SMA); Late Pleistocene (AFP) to Holocene fluvial and alluvial conglomerates and sands (SDE, FLP AFH). These outcrops exhibit variable thickness (between 20 and more than 100 m) and complex heteropic relationships (Pucci et al., 2015, 2019), which are also seen in the seismic data, especially along profiles B1 and B2 (see Figure 4a and Figures S4–S5 in Supporting Information S1).

Stratigraphic data from the two wells closer to the seismic profiles B1 and P1 ties to about 150 m deep our interpretation of the near-surface reflective features. LAqui-core well (Figure 3; Macrì et al., 2016) is located along

profile B1 at CMP 250 (Figures 4 and 7) and pierces our Units 3–5. Unit 5a corresponds to Units 1 and 2 of Macrì et al. (2016). Unit 5b and Units 4c can be related to Late-Middle Pleistocene palustrine and alluvial fan sediments drilled at 41–83 m and at 83–115 m (Units 3 and 4 of Macrì et al., 2016), respectively. Unit 3a might correspond to the palustrine sequence (related to the Early Pleistocene Scoppito-Madonna della Strada Unit, 1.3–1.7 Ma) drilled from 115 m to final depth. The deeper part of Unit 3a and Unit 3b have no borehole constraint. From the analysis of surface geology, we think that at least part of Unit 3a may be related to the outcropping lacustrine Pianola Unit, which according to Pucci et al. (2015, 2019) is older than the Scoppito-Madonna della Strada Unit, based on its stratigraphic position.

Borehole S1 (Figures 2 and 6), located 320 m to the southeast of profile P1, was drilled into a thick sequence of Early Pleistocene to Holocene alluvial fan deposits and encounters fractured limestones at 78 m depth, confirming the absence of Unit 2 in the Paganica sector of the Aterno Valley. Villani et al. (2017) correlate these limestones to the top of the BIS Formation, because borehole S1 is in the hanging wall of the Paganica Fault, exposing southwest-dipping beds of the BIS Formation in the footwall. Limestones encountered in this borehole are shallower than the top-basement as imaged on profile P1. As suggested by Villani et al. (2017), this may indicate a local northwest-dip of the top of Unit 1. This discrepancy can also be explained by the fact that seismic profile P1 is located near the Raiale riverbed, so that the underlying limestone substratum may have been subject to deep fluvial erosion.

The five seismo-stratigraphic units described above are dissected by several conjugate normal faults (drawn in black and red in Figures 4–6) mostly with moderate to high dip angle. Some of these normal faults only affect the Mesozoic-Tertiary basement, while others also dissect the continental sequence. Along the Paganica profiles, some of the younger fault strands reach the base of the Holocene (in red in Figure 6b) and show an overall good spatial correlation with the mapped tectonic structures (i.e., Mt. Caticchio and Mt. Bazzano faults) and with the coseismic surface ruptures originated by the 2009 Mw 6.1 L'Aquila earthquake (Figure 8: Boncio et al., 2010; Cinti et al., 2011; Iezzi et al., 2019; Vittori et al., 2011). Across the Bazzano profiles on the other hand, the majority of the interpreted faults affect the lowermost continental sequences and do not displace Unit 5, which according to our interpretation spans the final part of Middle Pleistocene to Holocene. The apparent dip-slip component for the individual fault segments, measured at the top of Unit 1 varies from a minimum of 5–10 m to a maximum of 80–90 m. Low-angle reverse faults (in red in Figure 4b) dissect Unit 1 and Unit 2 across profile B1. We interpret these thrusts as the relict expression of the late Miocene-early Pliocene compressive phase affecting this sector of the Apennines, as we further discuss in the following.

Additional information on the physical properties of basin infill come from results of the acoustic impedance inversion. Acoustic impedance is closely related to lithology, porosity, pore fill, and other factors. It is common to find robust empirical relationships between acoustic impedance and one or more of these rock properties (Buxton Latimer et al., 2000). Unfortunately, well log data are not available in Bazzano. Nevertheless, the results of acoustic impedance inversion shown in Figure 7b allow a qualitative yet meaningful assessment of porosity distribution in the Bazzano sub-basin, based on the reasonable assumption that in sedimentary basins low values of porosity are generally strongly correlated with high values of seismic impedance and vice-versa. In such environments, changes in acoustic impedance can pinpoint lithological or paleoenvironmental changes.

In particular, it is worth noting that an overall low seismic impedance (that we correlate to higher-porosity, i.e., Hp in Figure 7b) characterize the Holocene-to-Late-Pleistocene filling (i.e., Unit 5), while the Early to Middle-Pleistocene Unit 4 and 3 shows a gradual increase of acoustic impedance. Near the LAqui-core well, among a general low-impedance background, two bright, thin (i.e., ∼15–20 m thick) beds stand out with higher acoustic impedance and quite large continuity (i.e., ∼500 m: see Figure 7b CMP 180–380). Based on the well stratigraphy (Macri et al., 2016), we interpret these features as packages of lower porosity (i.e., Lp in Figure 7b) lacustrine deposits interbedded to higher-porosity (Hp) fluvial and alluvial fan sediments. Similar packages of thin beds with alternating higher and lower acoustic impedance and with even larger lateral continuity (i.e., almost the entire profile length) are found on profile B2 below the Aterno river (see Figure 7b).

Comparable alternating layers with lower/higher acoustic impedances (but thicker and with a higher absolute value) are found within the basement Units 1 and 2 (see Figure 7b: TWT > 0.3 s). This is also in agreement with the geological information, as large lithological variations are found in the outcrops of the Late Miocene marly

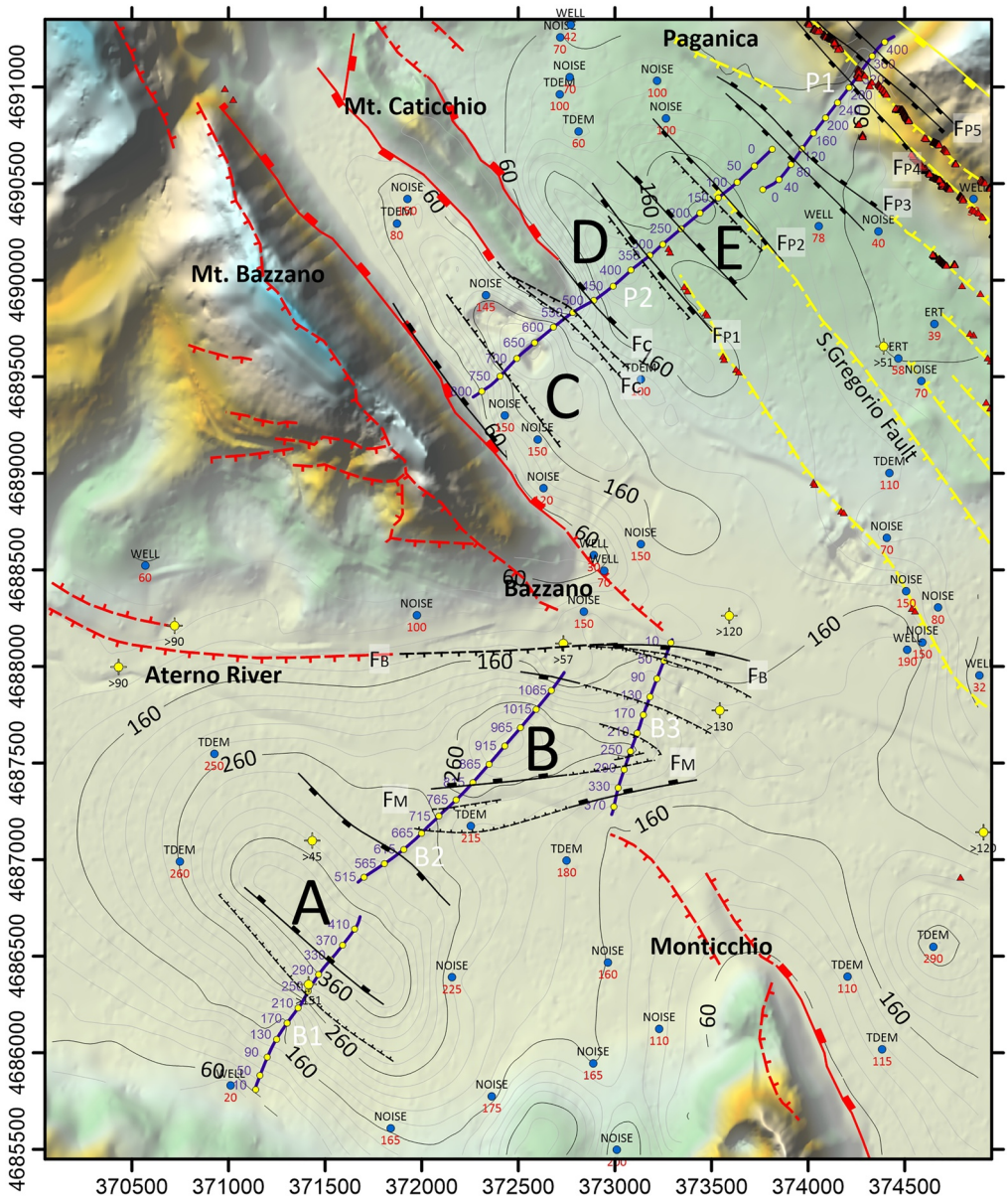

Figure 8. Contour map of the Meso-Cenozoic basement and inferred strike (in black) of the faults cutting the continental infill recognized in the seismic lines (dashed lines: presumed faults; barbs indicate the down-thrown side). The pattern of pre-Quaternary basement is estimated by spatial interpolation of (a) basement depths found along the seismic profiles; (b) outcrops of the pre-Quaternary basement in the study area; (c) punctual information from shallow boreholes reaching and not reaching the Meso-Cenozoic basement (yellow dots with cross); (d) geophysical surveys (blue dots: Civico et al., 2017; noise, ambient noise; TDEM, time-domain electromagnetic method; ERT, electric resistivity tomography). Basement morphology and proposed fault strikes are compared with: the main known structural trends (red); the fault strands activated during the 2009 event (yellow) and the surface ruptures occurred during the 2009 earthquake (red triangles) (from Boncio et al., 2010; Emergeo Working Group, 2010; Galli et al., 2010; Pucci et al., 2015, 2019).

limestones and arenaceous flysch that make up Unit 2, as well in the upper part of Mesozoic-Miocene marly and marly limestone sequence (Unit 1).

6. Discussion

The seismic profiles presented here reveal for the first time and with unprecedented resolution the structural and stratigraphic features of Paganica and Bazzano basins, which are key tectonic features in the region struck by the 2009 L'Aquila earthquake. Profiles B1 and B2, which provided the best-quality data, show with metric-to-decametric resolution features typical of lacustrine deposits (possibly equivalent to the Early Pleistocene Pianola Unit; see Section 3) alternated to several cycles of Early to Late Pleistocene alluvial fan and fluvial sediments (Galli et al., 2010; Giaccio et al., 2012) and locally dissected by active faults. Seismic reflection data depict the internal architecture of Bazzano basin, providing a clear picture of the progradation of the fans over the Middle Aterno Valley. In the Paganica basin, seismic data pinpoint a higher structural complexity due to the presence of a complex system of southwest-dipping normal faults with associated antithetic splays that controlled the deposition of Pleistocene coarse clastic deposits belonging to alluvial fan and fluvial sequences.

Overall, the five seismic profiles analyzed in this study show a complex topography of Meso-Cenozoic substratum, mostly due to a series of conjugate normal faults. In fact, there is a consistent match between the location of the normal faults and the large-scale steps in the top-substratum. Those steps are also associated with sharp lateral *Vp* changes reported by Villani et al. (2017). For these reasons, we think that extensional tectonics played a major role in the shaping the subsurface morphology of the two basins. Most of these normal faults affect part of the overlying sequence of continental deposits. We also detect some faults with clear evidence of very recent activity, as they displace the uppermost part of the shallowest Unit 5.

The structural map in Figure 8 shows the inferred strike of the most recent faults. The Paganica fault strikes are made consistent with the general northwest trend of the mapped faults and of the 2009 coseismic surface ruptures. Fault strikes on Bazzano have been interpolated, when possible, using the lateral offset observed between B2 and B3 and also using as constraint the strike of the mapped faults bounding the horsts of Monticchio and Bazzano. In Figure 8, we also present a contour map of the depth of the Meso-Cenozoic substratum in the Middle Aterno Valley, obtained by spatial interpolation of: (a) the top of basement depths (i.e., above Units 1 and 2) picked along the five profiles; (b) punctual basement depths from borehole data and geophysical surveys reported in Civico et al. (2017). The basement trend has been extrapolated farther away from the profiles using the outcrops of the Meso-Cenozoic substratum in the nearby mountains as a constraint.

From the analysis of this map and of the seismic profiles we infer that cumulative slip along Bazzano fault strands results in two depocenters (A and B in Figure 8), separated by a central horst. The southern depocenter "A" is ∼400 m deep, while the northern one, which is roughly located below the present-day location of the Aterno River, reaches a depth of ∼320 m below the ground. Lacustrine, alluvium and alluvial fan deposits, as shown on profiles B1 and B2 (Figure 4), fill these depocenters. Alluvial fans exhibit a sediment supply from different directions, with a prevailing feeding from the northeast, which is probably influenced by the accommodation space provided by the activation of different fault strands over time. It can be seen on the map of Figure 8 that we interpret fault F_M as a west-striking, north-dipping structure delimiting to the north Monticchio Horst. This fault and its conjugate pair F_B, that is, the southern tip of Bazzano horst, bound the secondary depocenter "B" of Bazzano basin, which is elongated in the west direction, thus dividing the Monticchio and Bazzano horsts. From the analysis of profile B2, F_M controls the overall depositional architecture of this sub-basin, with a total displacement of more than 100 m. Major reflector packages within Units 3b and 4b show indeed growth relationships that dip toward the depocenter and thin toward the northeast end of the basin. Growth relationships are evidenced by warped reflectors close to the F_M fault plane and onlapping relationships above unconformities.

In the map of Figure 8, the Paganica area is instead characterized by a shallower depth of the rugged substratum, which is dissected by a system of northwest-striking, conjugate normal faults. Seismic line P2 (Figure 6) shows indeed at least three depocenters, labeled as C, D, and E in Figure 8. Depocenter C is ∼240 m deep and is located between Mt. Bazzano and Mt. Caticchio, where the Meso-Cenozoic substratum outcrops ∼50–60 m to the northwest of the seismic profile. The central depocenter "D", set to the northeast of Mt. Caticchio, is bounded to the northeast by a ∼200 m wide buried horst whose top is found at ∼140 m b.g.l. The horst is delimited to the southwest by fault F_{P1} (Figure 6b). We note that the surface projection of F_{P1}, which is in good agreement with

the coseismic surface ruptures reported by Boncio et al. (2010), delineates a northwest-trending active fault splay in the hanging wall of the San Gregorio Fault (Figure 8).

The third ~220 m deep graben "E" is located south of Paganica village, and is bounded to the northeast by fault $F_{P2,}$ which is the northwest prolongation of the San Gregorio Fault (Boncio et al., 2010; Pucci et al., 2015; Villani et al., 2017). In our interpretation F_{P2}, rather than a single fault, represents a 125 m wide fault zone with a cumulative normal slip component, measured at the top of Unit 2, of at least 60 m. At the top of Unit 3b, the normal slip component reduces to 12–14 m. The increase of the slip downwards proves a syn-sedimentary activity of F_{P2}. Faulting in the uppermost Units 4 and 5 is not clear from the seismic image due to resolution limits: however, the close accord of F_{P2} with coseismic breaks described by Boncio et al. (2010) suggest that the uppermost fault termination is very shallow and may affect Unit 5 (dashed line in Figure 6).

Line P1 shows a general thinning of the continental deposits from southwest to northeast due to a shallower Meso-Cenozoic substratum dissected by active faults with a prevalent southwest dip such as the Paganica Fault (i.e., F_{P5}) and its main splay F_{P4}, with a few antithetic structures (i.e., F_{P3}). Faults F_{P4} and F_{P5} clearly cut the shallow deposits (Unit 3b) and the base of Unit 4b; they match with the main coseismic surface ruptures of the 2009 earthquake. Synsedimentary activity of these faults is indicated by the thickening of recent sediments in the hanging wall and by the cumulative vertical offset that increases with depth. For fault F_{P4}, which follows main surface ruptures observed after the mainshock, the cumulative vertical offset is about 20 m at the substratum top and between 5 and 10 m at the base of Unit 4b. A larger cumulative offset (about 30 m) of the carbonate substratum is produced by a synthetic splay of F_{P4}. The two structures define a complex, 50 m wide fault zone.

The Meso-Cenozoic substratum outcrops ~100 m to the northeast of P1. The internal architecture of alluvial deposits, predominant on P1, is not as visible as on the Bazzano lines; however, these deposits show a prevalent southwest progradation above the depocenters "C" and "E", which is consistent with the surface architecture of the alluvial deposits mapped in the area (Pucci et al., 2015, 2019). Sub-horizontal deposition and onlap terminations prevail on line P1.

Our interpolated depths for the Bazzano basin are in very good agreement with those of Florio et al. (2021), which are based on a constrained inversion of the gravity data. Their modeled Bazzano basin, with a west-northwest elongated shape and a maximum depth of ~360 m, is in accordance with our interpretation. Conversely, for the Paganica Basin, Florio et al. (2021) infer a maximum and constant depth of only ~100 m, which is much simpler and shallower than our findings (~220–240 m) and than those of Improta et al. (2012) and Villani et al. (2017). The Florio et al. (2021) estimate is also in disagreement with the top-bedrock map of Civico et al. (2017), which is based on interpolation of substratum depth evaluations from time-domain electro-magnetic sounding, electrical resistivity tomography, and single-station ambient vibration surveys. We note that the 2D deep electrical resistivity tomography model by Pucci et al. (2016), is also in agreement with our findings. The inversion results of Florio et al. (2021) in the Paganica basin may be biased by the juxtaposition of thick, and relatively high-density Pleistocene breccia and highly cemented alluvial fan conglomerates above the Meso-Cenozoic substratum. It is also worth noting that the resolution of the aerogravimetric data used by Florio et al. (2021) does not allow to retrieve the fine details of the complex Paganica basin.

A 400 m deep depocenter imaged in the southern part of the Bazzano basin is a key result of our survey when compared to the accurate stratigraphic information of the LAqui-core drilling. We remind that the borehole encountered reverse polarity, palustrine clays (Early Pleistocene in age) from 115 m to the bottom hole at 151 m depth; these fine solis were related to the Scoppito-Madonna della Strada Unit (1.3–1.8 Ma) outcropping to the west of the Bazzano basin (Macrì et al., 2016). Here, the good-quality seismic reflection data and the results of acoustic impedance inversion unravel, under the bottom-hole, 200–250 m of additional continental sediments (lacustrine, alluvial, and alluvial fan deposits). These deposits are certainly older, and possibly their upper part can be related to the Early Pleistocene Pianola Unit (similar in age to the >2.5 Ma old Limi di San Nicandro Formation, according to Cosentino et al., 2017 and Pucci et al., 2019). This finding is consistent with the tomographic survey of Improta et al. (2012) that defined a low-Vp zone (Vp = 1,500–2,500 m/s) about 150–200 m thick in the lower part of the basin.

In addition, the underlying Meso-Cenozoic substratum appears deformed by two reverse faults that gently dip westwards and possibly related to the Mt. Ocre regional thrust system (see Figure 1). The shallower thrust and its back-thrust seem to displace the basal part of the most ancient continental deposits (Unit 3b). Taken together,

all this information suggests a long-term polyphase evolution of the Bazzano basin that is more complex than previously hypothesized. Unfortunately, no direct dating of the lowermost continental sequence (Unit 3) is available. However, since it is carved in the outcropping Early Pleistocene Scoppito-Madonna della Strada and Pianola Units, an Early Pleistocene or possibly a Late Pliocene age is probable. This is also in accordance with reasonable long-term sedimentation rates inferred from the LAqui-core borehole (about 0.1 mm/yr), for which the nearly 300–350 m deep Unit 3 in the Bazzano basin may be as old as about 3–3.5 Myr. Accordingly, no evidence of contractional tectonics affecting the Quaternary Units 3a, 4, and 5 is found, in agreement with the local and regional geological setting (e.g., Cavinato & De Celles, 1999). Based on the hints of thrusting in the basal part of the continental succession beneath the southwestern sector of the Bazzano basin, we speculate that the most ancient continental deposits may have recorded the latest episode of shortening in this sector of the Apennines. Under this hypothesis, the Bazzano paleo-basin was emplaced on top of thrust sheets of the Mio-Pliocene orogeny, near the end of the main contractional phase, and was later controlled by normal faulting since the late Pliocene-Early Pleistocene. To validate our hypothesis, new high-resolution seismic profiles are needed to map the 3-D geometry of the thrust structures buried beneath the Bazzano basin. In addition, direct dating from new and deeper boreholes can provide further insights into the long-term tectonic evolution of this key area.

7. Conclusions

The five high-resolution seismic reflection profiles targeting the Bazzano and Paganica basins in the Middle-Aterno Valley allowed us to develop an informative seismic image cutting across the shallow strands of the Paganica-San Demetrio Fault, the causative fault of the 2009 (Mw 6.1) earthquake and to expose the basin structure with unprecedented resolution. By combining seismic amplitudes with the energy and similarity attributes and with post-stack acoustic impedance for the Bazzano profiles, we were able to provide a reliable and consistent interpretation of a fault-controlled and rather complex basin. The imaged basins show several depocenters carved in the Meso-Cenozoic substratum and filled by reflective packages with seismo-stratigraphic features typical of alluvial fans, alluvial, lacustrine and palustrine sediments of late Pliocene to Holocene age. The inferred strike of faults offsetting continental infill deposits suggests that the Paganica and Bazzano basins have different structure and evolution. The Bazzano basin is older and likely originated at the end of Pliocene. We speculate that the basal part of its continental succession was deformed by a Late Pliocene compressional phase that was later overprinted by west-striking normal faulting. Our hypotheses are based on two key observations: (a) the large thickness of the basin infill (400 m) if compared to the Early Pleistocene age (1.3–1.8 Ma) of palustrine deposits drilled at 151 m depth in the LAqui-core scientific drilling (Macrì et al., 2016); (b) the hints of reverse faulting that seem to affect the lowermost sequence filling the western depocenter of the Bazzano basin (possibly 3–3.5 Ma in age). Conversely, the Paganica basin appears to be exclusively controlled by northwest-trending Quaternary normal faults, that are responsible for the current seismicity of the region.

Comparison with tomography *Vp* models of Improta et al. (2012) and Villani et al. (2017) (see Figures S8 and S9 in Supporting Information S1) shows that at Bazzano, where the basin filling is on average less coarse and more homogeneous, the seismic reflection imaging is more effective than seismic tomography in depicting the structural and stratigraphic features and in delineating the substrate morphology. Conversely, at Paganica, due to the occurrence of coarser sediments coupled to a higher structural complexity and a higher level of seismic noise, the quality of the reflection images is lower than in Bazzano and the combination of the two techniques (i.e., seismic reflection and seismic tomography) has its advantages in better discriminating the substrate. The high-quality of the seismic imaging achieved at Bazzano represents a leap forward in the knowledge of the substrate geometry and internal architecture of the basin compared to previous studies. For instance, the seismic tomography imaging of Improta et al. (2012), which constituted the best result obtained prior to our study, allowed to define only the large-scale structure of the basin.

Moreover, post-stack acoustic impedance inversion provides additional elements for the interpretation of the Bazzano basin. Our article is probably the first example of application of this technique to interpret shallow high-resolution data acquired in fault-controlled, intramontane basins. Overall, this study provides solid and additional evidence that high-resolution seismic reflection imaging should be considered as a primary geophysical tool for subsurface basin imaging and active faults detection in complex tectonic scenarios.

Conflict of Interest

The authors declare no conflicts of interest relevant to this study.

Data Availability Statement

The seismic reflection data supporting the conclusions are available in the repository available at the following link: https://doi.org/10.6084/m9.figshare.14637789.v3.

Acknowledgments
This research has been funded by the Project INGV-DPC S5 07–09 "*Test sites per il monitoraggio multidisciplinare di dettaglio*" W.P. 4.5 (team 0371.050, UR8, P.I.: L. Improta) and by the INGV Project *Pianeta Dinamico*, Task S2 2022 (code C.U.P. D53J19000170001), funded by the MUR: legge n. 145/2018. The authors thank Massimiliano Barchi; Francesco Mirabella, William Stephenson, and an anonymous reviewer for their very helpful comments that allowed us to improve the quality of this work. The authors acknowledge support of this work via a Landmark Grant Program to the University of Napoli "Federico II" and to the INGV by Halliburton Software and Services, a Halliburton Company. The authors also acknowledge support of this work to dGB Earth Science via an academic license agreement for OpendTect Pro® software to the University "Federico II". Open Access Funding provided by Universita degli Studi di Napoli Federico II within the CRUI-CARE Agreement.

References

Akinci, A., Galadini, F., Pantosti, D., Petersen, M., Malagnini, L., & Perkins, D. (2009). Effect of time dependence on probabilistic seismic-hazard maps and deaggregation for the central Apennines, Italy. *Bulletin of the Seismological Society of America*, *99*(2A), 585–610. https://doi.org/10.1785/0120080053

Atzori, S., Hunstad, I., Chini, M., Salvi, S., Tolomei, C., Bignami, C., et al. (2009). Finite fault inversion of DInSAR coseismic displacement of the 2009 L'Aquila earthquake (central Italy). *Geophysical Research Letters*, *36*, L15305. https://doi.org/10.1029/2009GL039293

Baccheschi, P., De Gori, P., Villani, F., Trippetta, F., & Chiarabba, C. (2020). The preparatory phase of the Mw 6.1 2009 L'Aquila normal faulting earthquake traced by foreshocks time-lapse tomography. *Geology*, *48*(1), 49–55. https://doi.org/10.1130/G46618.1

Bagnaia, R., D'Epifanio, A., & Sylos Labini, S. (1992). *Aquila and subaequan basins: An example of Quaternary evolution in central Apennines, Italy* (pp. 187–209). Quaternaria Nova, II.

Balasco, M., Alli, P. G., Iocoli, A. G., Ueguen, E. G., Apenna, V. L., Errone, A. P., et al. (2011). Deep geophysical electromagnetic section across the Middle Aterno Valley (central Italy): Preliminary results after the April 6, 2009 L'Aquila earthquake. *Bollettino di Geofisica Teorica ed Applicata*, *52*, 443–455.

Barchi, M. R., Carboni, F., Michele, M., Ercoli, M., Giorgetti, C., & Porreca, M. (2021). The influence of subsurface geology on the distribution of earthquakes during the 2016–2017 Central Italy seismic sequence. *Tectonophysics*, *807*, 228797. https://doi.org/10.1016/j.tecto.2021.228797

Bertini, T., & Bosi, C. (1993). La tettonica quaternaria della conca di Fossa—San Demetrio (L'Aquila). *Il Quaternario Italian Journal of Quaternary Sciences*, *6*(2), 293–314.

Blumetti, A. M., Di Manna, P., Comerci, V., Guerrieri, L., & Vittori, E. (2017). Paleoseismicity of the San Demetrio ne' Vestini fault (L'Aquila basin, central Italy): Implications for seismic hazard. *Quaternary International*, *451*, 129–142. https://doi.org/10.1016/j.quaint.2016.12.039

Boncio, P., Lavecchia, G., & Pace, B. (2004). Defining a model of 3-D seismogenic sources for seismic hazard assessment applications: The case of central Apennines (Italy). *Journal of Seismology*, *8*(3), 407–425.

Boncio, P., Pizzi, A., Brozzetti, F., Pomposo, G., Lavecchia, G., Di Naccio, D., & Ferrarini, F. (2010). Coseismic ground deformation of the April 6, 2009 L'Aquila earthquake (central Italy, Mw 6.3). *Geophysical Research Letters*, *37*, L06308. https://doi.org/10.1029/2010GL042807

Bosi, C., & Bertini, T. (1970). Geologia della media valle dell'Aterno. *Mémoires de la Société géologique de France*, *9*, 719–777.

Bosi, C., Galadini, F., Giaccio, B., Messina, P., & Sposato, A. (2003). Plio-Quaternary continental deposits in the Latium-Abruzzi Apennines: The correlation of geological events across different intermontane basins. *Il Quaternario Italian Journal of Quaternary Sciences*, *16*(1Bis), 55–76.

Bosi, C., & Messina, P. (1991). Ipotesi di correlazione fra successioni morfo-litostratigrafiche plio-pleistoceniche nell'Appennino Laziale-Abruzzese. *Studi Geologici Camerti*, *1991/2*, 257–263.

Bruno, P. P. G., Berti, C., & Pazzaglia, F. J. (2019). Accommodation, slip inversion, and segmentation in a province-scale shear zone from high-resolution, densely spaced, wide-aperture seismic profiling, Centennial Valley, MT, USA. *Scientific Reports*, *9*, 9214. https://doi.org/10.1038/s41598-019-45497-1

Bruno, P. P. G., Castiello, A., Villani, F. & Improta, L. (2013). High-resolution densely spaced wide-aperture seismic profiling as a tool to aid seismic hazard assessment of fault-bounded intramontane basins: Application to Vallo di Diano, Southern Italy. *Bulletin of the Seismological Society of America*, *103*(3), 1969–1980. https://doi.org/10.1785/0120120071

Bruno, P. P. G., DuRoss, C. B., & Kokkalas, S. (2017). High-resolution seismic profiling reveals faulting associated with the 1934 Ms 6.6 Hansel Valley earthquake (Utah, USA). *The Geological Society of America Bulletin*, *129*, 1227–1240. https://doi.org/10.1130/B31516.1

Buttinelli, M., Petracchini, L., Maesano, F. E., D'Ambrogi, C., Scrocca, D., Marino, M., et al. (2021). The impact of structural complexity, fault segmentation, and reactivation on seismotectonics: Constraints from the upper crust of the 2016–2017 central Italy seismic sequence area. *Tectonophysics*, *810*, 228861. https://doi.org/10.1016/j.tecto.2021.228861

Buxton Latimer, R., Davison, R., & Van Riel, P. (2000). An interpreter's guide to understanding and working with seismic-derived acoustic impedance data. *The Leading Edge*, *19*(3), 242–256. https://doi.org/10.1190/1.1438580

Cavinato, G. P., & De Celles, P. G. (1999). Extensional basins in the tectonically bimodal central Apennines fold-thrust belt, Italy: Response to corner flow above a subducting slab in retrograde motion. *Geology*, *27*(10), 955–958.

Centamore, E., Crescenti, U., Dramis, F., Bigi, S., Fumanti, F., Rusciadelli, G., et al. (2006). *Note illustrative della Carta geologica d'Italia alla scala 1:50.000, Foglio 359 "L'Aquila"* (p. 128). Firenze: APAT-Servizio Geologico d'Italia e Regione Abruzzo-Servizio Difesa del Suolo, S.EL.CA.

Cesi, C., Di Filippo, M., Di Nezza, M., & Ferri, M. (2010). Caratteri gravimetrici della media Valle del Fiume Aterno. In Gruppo di Lavoro MS-AQ (Ed.), *Microzonazione sismica per la ricostruzione dell'area aquilana. Regione Abruzzo—Dipartimento della Protezione Civile* (Vol. 3). L'Aquila.

Chiarabba, C., Amato, A., Anselmi, M., Baccheschi, P., Bianchi, I., Cattaneo, M., et al. (2009). The 2009 L'Aquila (central Italy) Mw 6.3 earthquake: Main shock and aftershocks. *Geophysical Research Letters*, *36*, L18308. https://doi.org/10.1029/2009GL039627

Chiaraluce, L. (2012). Unraveling the complexity of Apenninic extensional fault systems: A review of the 2009 L'Aquila earthquake (central Apennines, Italy). *Journal of Structural Geology*, *42*, 2–18.

Chiaraluce, L., Valoroso, L., Piccinini, D., Di Stefano, R., & De Gori, P. (2011). The anatomy of the 2009 L'Aquila normal fault system (central Italy) imaged by high-resolution foreshock and aftershock locations. *Journal of Geophysical Research*, *116*, B12311. https://doi.org/10.1029/2011JB008352

Chopra, S., & Marfurt, K. J. (2005). Seismic attributes—A historical perspective. *Geophysics*, *70/5*. https://doi.org/10.1190/1.2098670

Cinti, F. R., Pantosti, D., De Martini, P. M., Pucci, S., Civico, R., Pierdominici, S., et al. (2011). Evidence for surface faulting events along the Paganica Fault prior to the April 6, 2009 L'Aquila earthquake (central Italy). *Journal of Geophysical Research*, *116*(B7), 2156–2202.

Cirella, A., Piatanesi, A., Tinti, E., Chini, M., & Cocco, M. (2012). Complexity of the rupture process during the 2009 L'Aquila, Italy, earthquake. *Geophysical Journal International*, *190*, 607–621.

Civico, R., Sapia, V., Di Giulio, G., Villani, F., Pucci, S., Baccheschi, P., et al. (2017). Geometry and evolution of a fault-controlled Quaternary basin by means of TDEM and single-station ambient vibration surveys: The example of the 2009 L'Aquila earthquake area, central Italy. *Journal of Geophysical Research: Solid Earth*, *122*(3), 2236–2259. https://doi.org/10.1002/2016JB013451

Cosentino, D., Asti, R., Nocentini, M., Gliozzi, E., Kotsakis, T., Mattei, M., et al. (2017). New insights into the onset and evolution of the central Apennine extensional intermontane basins based on the tectonically active L'Aquila basin (central Italy). *GSA Bulletin*, *129*(9–10), 1314–1336. https://doi.org/10.1130/B31679.1

Cosentino, D., Cipollari, P., Marsili, P., & Scrocca, D. (2010). Geology of the central Apennines: A regional review. In M.Beltrando, A.Peccerillo, M.Mattei, S.Conticelli, & C.Doglioni (Eds.), *The geology of Italy. Journal of the virtual explorer*. Electronic Edition. Retrieved from http://virtualexplorer.com.au/article/2009/223/apennines-review

Cowie, P. A., & Roberts, G. P. (2001). Constraining slip rates and spacings for active normal faults. *Journal of Structural Geology*, *23*, 1901–1915.

D'Agostino, N., Jackson, J. A., Dramis, F., & Funiciello, R. (2001). Interactions between mantle upwelling, drainage evolution, and active normal faulting: An example from the central Apennines (Italy). *Geophysical Journal International*, *147*(2), 475–497.

D'Amico, S., Koper, K. D., Herrmann, R. B., Akinci, A., & Malagnini, L. (2010). Imaging the rupture of the Mw 6.3 April 6, 2009 L'Aquila, Italy earthquake using back-projection of teleseismic *P* waves. *Geophysical Research Letters*, *37*, L03301. https://doi.org/10.1029/2009GL042156

Emergeo Working Group. (2010). Evidence for surface rupture associated with the Mw 6.3 L'Aquila earthquake sequence of April 2009 (central Italy). *Terra Nova*, *22*(1), 43–51. https://doi.org/10.1111/j.1365-3121.2009.00915.x

Emery, D., Myers, K. J., Bertram, G., Griffiths, C., Milton, N., Reynolds, T., et al. (Eds.). (1996). *Sequence stratigraphy* (p. 291). Blackwell Science Ltd.

Ercoli, M., Forte, E., Porreca, M., Carbonell, R., Pauselli, C., Minelli, G., & Barchi, M. R. (2020). Using seismic attributes in seismotectonic research: An application to the Norcia Mw D 6:5 earthquake (October 30, 2016) in central Italy. *Solid Earth*, *11*, 329–348. https://doi.org/10.5194/se-11-329-2020

Florio, G., Milano, M., & Cella, F. (2021). Gravity basement-depth mapping in seismogenic, fault-controlled basins: The case of the Middle Aterno Valley (Central Italy). *Tectonophysics*, *817*, 229044. https://doi.org/10.1016/j.tecto.2021.229044

Galadini, F. (1999). Pleistocene change in the central Apennine fault kinematics, a key to decipher active tectonics in central Italy. *Tectonics*, *18*, 877–894.

Galadini, F., & Galli, P. (2000). Active tectonics in the central Apennines (Italy)—Input data for seismic hazard assessment. *Natural Hazards*, *22*, 225–270.

Galadini, F., & Messina, P. (2001). Plio-Quaternary changes of the normal fault architecture in the central Apennines (Italy). *Geodinamica Acta*, *14*, 321–344.

Galadini, F., & Messina, P. (2004). Early-middle Pleistocene eastward migration of the Abruzzi Apennine (central Italy) extensional domain. *Journal of Geodynamics*, *37*, 57–81.

Galbraith, J. M., & Millington, G. F. (1978). *Low-frequency recovery in the inversion of seismograms* (pp. 30–39). Calgary.

Galli, P. A., Galadini, F., & Pantosti, D. (2008). Twenty years of paleoseismology in Italy. *Earth-Science Reviews*, *88*(1), 89–117.

Galli, P. A., Giaccio, B., & Messina, P. (2010). The 2009 central Italy earthquake seen through 0.5 Myr long tectonic history of the L'Aquila faults system. *Quaternary Science Reviews*, *29*(27–28), 3768–3789.

Galli, P. A., Giaccio, B., Messina, P., Peronace, E., & Zuppi, G. M. (2011). Palaeoseismology of the L'Aquila faults (central Italy, 2009, Mw 6.3 earthquake): Implications for active fault linkage. *Geophysical Journal International*, *187*(3), 1119–1134.

Gardner, G. H. F., Gardner, L. W., Gregory, A. R. (1974). Formation velocity and density—The diagnostic basics for stratigraphic traps. *Geophysics*, *93*(6), 759–791. ISSN (online):1942-2156.

Ghisetti, F., Barchi, M., Bally, A. W., Moretti, I., & Vezzani, L. (1993). Conflicting balanced structural sections across the central Apennines (Italy): Problems and implications, generation, accumulation and production of Europe's hydrocarbon. In A. M.Spencer (Ed.), *Special Publication of the European Association of Petroleum Geoscientists* (Vol. 3, pp. 219–231).

Ghisetti, F., & Vezzani, L. (1999). Depths and modes of Pliocene-Pleistocene crustal extension of the Apennines (Italy). *Terra Nova*, *11*, 67–72.

Giaccio, B., Galli, P., Messina, P., Peronace, E., Scardia, G., Sottili, G., et al. (2012). Fault and basin depocenter migration over the last 2 Ma in the L'Aquila 2009 earthquake region, central Italian Apennines. *Quaternary Science Reviews*, *56*, 69–88.

Giocoli, A., Galli, P., Giaccio, B., Lapenna, V., Messina, P., Peronace, E., et al. (2011). Electrical resistivity tomography across the Paganica-San Demetrio fault system (L'Aquila 2009 earthquake). *Bollettino di Geofisica Teorica Applicata*, *52*, 457–469.

Gold, R. D., Stephenson, W. J., Briggs, R. W., DuRoss, C. B., Kirby, E., Woolery, E., et al. (2020). Seismic reflection imaging of the low-angle Panamint normal fault system, eastern California. *Journal of Geophysical Research: Solid Earth*, *125*(11), e2020JB020243.

Gregory, A. R. (1977). Aspects of rock physics from laboratory and log data that are important to seismic interpretation: Section 1. Fundamentals of stratigraphic interpretation of seismic data. In C. E.Payton (Ed.), *Seismic stratigraphy—Applications to hydrocarbon exploration* (Vol. 26). AAPG MEMOIR. https://doi.org/10.1306/M26490

Haberland, C., Gibert, L., Jurado, M. J., Stiller, M., Baumann-Wilke, M., Scott, G., & Mertz, D. F. (2017). Architecture and tectono-stratigraphic evolution of the intramontane Baza Basin (Bétics, SE-Spain): Constraints from seismic imaging. *Tectonophysics*, *709*, 69–84. ISSN 0040-1951.

Herrmann, R. B., Malagnini, L., & Munafo, I. (2011). Regional moment tensors of the 2009 L'Aquila earthquake sequence. *Bulletin of the Seismological Society of America*, *101*, 975–993.

Iezzi, F., Roberts, G., Walker, J. F., & Papanikolaou, I. (2019). Occurrence of partial and total coseismic ruptures of segmented normal fault systems: Insights from the central Apennines, Italy. *Journal of Structural Geology*, *126*, 83–99. https://doi.org/10.1016/j.jsg.2019.05.003

Improta, L., Villani, F., Bruno, P. P., Castiello, A., De Rosa, D., Varriale, F., et al. (2012). High-resolution controlled-source seismic tomography across the Middle Aterno basin in the epicentral area of 2009, Mw 6.3, L'Aquila earthquake (central Apennines, Italy). *Italian Journal of Geosciences*, *131*(3), 373–388.

Latimer, R. B., Davidson, R., & Van Riel, P. (2020). An interpreter's guide to understanding and working with seismic-derived acoustic impedance data. *The Leading Edge*, *19*(3), 242–256.

Latimer, R. B., Davison, R., & Riel, P. V. (2000). An interpreter's guide to understanding and working with seismic-derived acoustic impedance data. *The Leading Edge*, *19*, 242–256.

Lavecchia, G., Brozzetti, F., Barchi, M., Menichetti, M., & Keller, J. V. A. (1994). Seismotectonic zoning in east-central Italy deduced from an analysis of the Neogene to present deformations and related stress fields. *The Geological Society of America Bulletin*, *106*, 1107–1120.

Lavecchia, G., Ferrarini, F., Brozzetti, F., De Nardis, R., Boncio, P., & Chiaraluce, L. (2012). From surface geology to aftershock analysis: Constraints on the geometry of the L'Aquila 2009 seismogenic fault system. *Italian Journal of Geosciences*, *131*(3), 330–347.

Machette, M., Haller, K., & Wald, L. (2004). *Quaternary fault and fold database for the Nation*, (pp. 2004–3033). United States Geological Survey Fact Sheet.

Macrì, P., Smedile, A., Speranza, F., Sagnotti, L., Porreca, M., Mochales, & Russo Ermolli, T. E. (2016). Analysis of a 150 m sediment core from the coseismic subsidence depocenter of the 2009 Mw = 6.1 L'Aquila earthquake (Italy): Implications for Holocene-Pleistocene tectonic subsidence rates and for the age of the seismogenic Paganica Fault system. *Tectonophysics*, *687*, 180–194.

Malinverno, A., & Ryan, W. B. F. (1986). Extension in the Tyrrhenian Sea and shortening in the Apennines as result of arc migration driven by sinking of the lithosphere. *Tectonics*, *5*(2), 227–245.

Mancini, M., Cavuoto, G., Pandolfi, L., Petronio, C., Salari, L., & Sardella, R. (2012). Coupling infill history and mammal biochronology in a Pleistocene intramontane basin: The case of western L'Aquila basin (central Apennines, Italy). *Quaternary International*, *267*, 62–77. https://doi.org/10.1016/j.quaint.2011.03.020

Marfurt, K., Kirlin, R. L., Farmer, S. L., & Bahorich, M. S. (1998). 3-D seismic attributes using a semblance-based coherency algorithm. *Geophysics*, *63*(4), 1150–1165. https://doi.org/10.1190/1.1444415

Minelli, L., Speranza, F., Nicolosi, I., D'Ajello Caracciolo, F., Carluccio, R., Chiappini, S., et al. (2018). Aeromagnetic investigation of the central Apennine seismogenic zone (Italy): From basins to faults. *Tectonics*, *37*. https://doi.org/10.1002/2017TC004953

Morewood, N. C., & Roberts, G. P. (2000). The geometry, kinematics and rates of deformation within an en echelon normal fault segment boundary, central Italy. *Journal of Structural Geology*, *22*, 1027–1047.

Moro, M., Gori, S., Falcucci, E., Saroli, M., Galadini, F., & Salvi, S. (2013). Historical earthquakes and variable kinematic behavior of the 2009 L'Aquila seismic event (central Italy) causative fault, revealed by paleoseismological investigations. *Tectonophysics*, *583*, 131–144.

Oldenburg, D. W., Scheuer, T., & Levy, S. (1983). Recovery of the acoustic impedance from reflection seismograms. *Geophysics*, *48*(10). https://doi.org/10.1190/1.1440186

Operto, S., Ravaut, C., Improta, L., Virieux, J., Herrero, A., & Dell'Aversana, P. (2004). Quantitative imaging of complex structures from dense wide-aperture seismic data by multiscale traveltime and waveform inversions: A case study. *Geophysical Prospecting*, *52*(6), 625–651.

Pace, B., Peruzza, L., Lavecchia, G., & Boncio, P. (2006). Layered seismogenic source model and probabilistic seismic-hazard analyses in Central Italy. *Bulletin of the Seismological Society of America*, *96*(1), 107–132.

Papanikolaou, I. D., Foumelis, M., Paracharidis, E. L., Lekkas, J., & Fountoulis, G. (2010). Deformation pattern of the April 6–7, 2009, $M = 6.3$ and Mw 5.6 earthquakes in L'Aquila (central Italy) revealed by ground and space observations. *Natural Hazards and Earth System Sciences*, *10*, 73–87.

Patacca, E., Sartori, R., & Scandone, P. (1990). Tyrrhenian basin and Apenninic arcs: Kinematic relations since Late Tortonian times. *Memorie della Societa Geologica Italiana*, *45*(1), 425–451.

Patruno, S., & Scisciani, V. (2021). Testing normal fault growth models by seismic stratigraphic architecture: The case of the Pliocene-Quaternary Fucino Basin (central Apennines, Italy). *Basin Research*, *33*, 2118–2156. https://doi.org/10.1111/bre.12551

Pizzi, A., Di Domenica, A., Gallovič, F., Luzi, L., & Puglia, R. (2017). Fault segmentation as constraint to the occurrence of the main shocks of the 2016 central Italy seismic sequence. *Tectonics*, *36*, 2370–2387. https://doi.org/10.1002/2017TC004652

Pizzi, A., & Galadini, F. (2009). Pre-existing cross-structures and active fault segmentation in the northern-central Apennines (Italy). *Tectonophysics*, *476*, 304–319.

Pucci, S., Civico, R., Villani, F., Ricci, T., Delcher, E., Finizola, A., et al. (2016). Deep electrical resistivity tomography along the tectonically active Middle Aterno Valley (2009 L'Aquila earthquake area, central Italy). *Geophysical Journal International*, *207*, 967–982.

Pucci, S., Villani, F., Civico, R., Di Naccio, D., Porreca, M., Benedetti, L., et al. (2019). Complexity of the 2009 L'Aquila earthquake causative fault system (Abruzzi Apennines, Italy) and effects on the Middle Aterno Quaternary basin arrangement. *Quaternary Science Reviews*, *213*, 30–66. https://doi.org/10.1016/j.quascirev.2019.04.014

Pucci, S., Villani, F., Civico, R., Pantosti, D., Del Carlo, P., Smedile, A., et al. (2015). Quaternary geology map of the Middle Aterno Valley, 2009 L'Aquila earthquake area (Abruzzi Apennines, Italy). *Journal of Maps*, *11*(5), 689–697.

Roberts, G. P., Cowie, P., Papanikolou, I., & Michetti, A. M. (2004). Fault scaling relationships, deformation rates, and seismic hazards: An example from the Lazio-Abruzzo Apennines, central Italy. *Journal of Structural Geology*, *26*, 377–398.

Roberts, G. P., Michetti, A., Cowie, P. A., Morewood, N. C., & Papanikolaou, I. (2002). Fault slip-rate variations during crustal-scale strain localization, central Italy. *Geophysical Research Letters*, *29*(8), 9-1–9-4.

Roberts, G. P., Raithatha, B., Sileo, G., Pizzi, A., Pucci, S., Walker, J. F., et al. (2010). Shallow subsurface structure of the April 6, 2009 Mw 6.3 L'Aquila earthquake surface rupture at Paganica, investigated with ground-penetrating radar. *Geophysical Journal International*, *183*, 774–790.

Rovida, A., Camassi, R., Gasperini, P., & Stucchi, M. (Eds.). (2011). *CPTI11, the 2011 version of the parametric catalog of Italian Earthquakes*. https://doi.org/10.6092/INGV.IT-CPTI11

Scognamiglio, L., Tinti, E., Michelini, A., Dreger, D. S., Cirella, A., Cocco, M., et al. (2010). Fast determination of moment tensors and rupture history: What has been learned from the April 6, 2009 L'Aquila earthquake sequence. *Seismological Research Letters*, *81*(6), 892–906.

Stephenson, W. J., Frary, R. N., Louie, J., & Odum, J. K. (2013). Quaternary extensional growth folding beneath Reno, Nevada, imaged by urban seismic profiling. *Bulletin of the Seismological Society of America*, *103*(5), 2921–2927. https://doi.org/10.1785/012012031

Tarquini, S., Isola, I., Favalli, M., & Battistini, A. (2007). TINITALY, a digital elevation model of Italy with a 10 meters cell size (Version 1.0). [Data Set]. Istituto Nazionale di Geofisica e Vulcanologia (INGV). https://doi.org/10.13127/TINITALY/1.0

Tertulliani, A., Rossi, A., Cucci, L., & Vecchi, M. (2009). L'Aquila (central Italy) earthquakes: The predecessors of the April 6, 2009 event. *Seismological Research Letters*, *80*(6), 1008–1013.

Valoroso, L., Chiaraluce, L., Piccinini, D., Di Stefano, R., Schaff, D., & Waldhauser, F. (2013). Radiography of a normal fault system by 64,000 high-precision earthquake locations: The 2009 L'Aquila (central Italy) case study. *Journal of Geophysical Research*, *118*, 1156–1176.

Veeken, P. C. H. (2007). Seismic stratigraphy, basin analysis and reservoir characterization. *Handbook of geophysical exploration* (p. 509). Elsevier. ISBN 9780080453118.

Vezzani, L., Festa, A., & Ghisetti, F. (2010). Geology and tectonic evolution of the central-southern Apennines, Italy. *Geological Society of America Special Paper*, *469*, 58.

Vezzani, L., & Ghisetti, F. (1998). *Carta geologica dell'Abruzzo, scale 1:100,000*. Firenze: S.EL.CA.

Villani, F., Improta, L., Pucci, S., Civico, R., Bruno, P. P. G., & Pantosti, D. (2017). Investigating the architecture of the Paganica Fault (2009 Mw 6.1 earthquake, central Italy) by integrating high-resolution multiscale refraction tomography and detailed geological mapping. *Geophysical Journal International*, *208*, 403–423.

Villani, F., Maraio, S., Bruno, P. P., Improta, L., Wood, K., Pucci, S., et al. (2021). High-resolution seismic profiling in the hanging wall of the southern fault section ruptured during the 2016 Mw 6.5 central Italy earthquake. *Tectonics*, *40*(9), e2021TC006786. https://doi.org/10.1029/2021TC006786

Villani, F., Tulliani, V., Sapia, V., Fierro, E., Civico, R., & Pantosti, D. (2015). Shallow subsurface imaging of the Piano di Pezza active normal fault (central Italy) by high-resolution refraction and electrical resistivity tomography coupled with time-domain electromagnetic data. *Geophysical Journal International*, *203*(3), 1482–1494. https://doi.org/10.1093/gji/ggv399

Vittori, E., Blumetti, A. M., Comerci, V., Guerrieri, L., Esposito, E., Michetti, A. M., et al. (2011). Surface faulting of the April 6, 2009 Mw 6.3 L'Aquila earthquake in central Italy. *Bulletin of the Seismological Society of America*, *101*(4), 1507–1530.

References From the Supporting Information

Debeye, H. W. J., & Van Riel, P. (1990). Lp-norm deconvolution. *Geophysical Prospecting*, *38*(4).

Deidda, G. P., Battaglia, E., & Heilmann, Z. (2012). Common-reflection-surface imaging of shallow and ultrashallow reflectors. *Geophysics*, *77*(4), B177–B185.

Garabito, G., Stoffa, P. L., Lucena, L. S., & Cruz, J. C. (2012). Part I-CRS stack: Global optimization of the 2D CRS-attributes. *Journal of Applied Geophysics*, *85*, 92–101.

Gulunay, N. (1986). *F-X decon and the complex Wiener prediction filter for random noise reduction on stacked data*. Houston: 56th SEG Annual Meeting. *Expanded Abstracts*POS 2.10.

Jäger, R., Mann, J., Höcht, G., & Hubral, P. (2001). Common-reflection-surface stack: Image and attributes. *Geophysics*, *66*(1).

Lawton, D. C. (1989). Computation of refraction static corrections using first-break traveltime differences. *Geophysics*, *54*, 1289–1296.

Levin, S. A. (1989). Surface-consistent deconvolution. *Geophysics*, *54*, 1123–1133.

Levy, S., & Fullagar, P. K. (1981). Reconstruction of a sparse spike train from a portion of its spectrum and application to high-resolution deconvolution. *Geophysics*, *46*(9).

Mann, J., Jäger, R., Müller, T., Höcht, G., & Hubral, P. (1999). Common-reflection-surface stack—A real data example. *Journal of Applied Geophysics*, *42*(3), 301–318.

Müller, T. (1998). Common reflection surface stack versus NMO/stack and NMO/DMO stack. *Sixty EAGE Conference & Exhibition*.

Neidell, N. S., & Taner, M. T. (1971). Semblance and other coherency measures for multichannel data. *Geophysics*, *36*, 482–497. https://doi.org/10.1190/1.1440186

Palmer, D. (1980). *The generalized reciprocal method of seismic refraction interpretation*. Tulsa, OK: Society of Exploration Geophysicists.

Ronen, J., & Claerbout, J. F. (1985). Surface-consistent residual statics estimation by stack-power maximization. *Geophysics*, *50*, 2759–2767. https://doi.org/10.1190/1.1441896

Taner, M. T., Koehler, F., & Sheriff, R. E. (1981). Surface consistent corrections. *Geophysics*, *46*, 17–22. https://doi.org/10.1190/1.1441133

Yilmaz, O. (2001). Seismic data analysis. *SEG, Tulsa, Investigations in Geophysics 10*, *2*, 1000.